Electronic Thesis and Dissertation Repository

3-28-2017 12:00 AM

Hsp90 and its Co-chaperones Modify TDP-43 Localization, Aggregation, and Toxicity

Lilian T. Lin, *The University of Western Ontario*

Supervisor: Dr. Martin Duennwald, *The University of Western Ontario*
A thesis submitted in partial fulfillment of the requirements for the Master of Science degree in Pathology
© Lilian T. Lin 2017

Follow this and additional works at: https://ir.lib.uwo.ca/etd

Part of the Molecular Genetics Commons, and the Nervous System Diseases Commons

Recommended Citation

Abstract

Amyotrophic lateral sclerosis (ALS) is a neurodegenerative disease associated with protein misfolding and protein aggregation. In particular, the TAR DNA-binding protein (TDP-43) is often found in the pathological inclusions in neurons of ALS patient brains and spinal cords. This phenomenon is known as TDP-43 proteinopathy, the mislocalization of TDP-43 from the cell nucleus and the formation of aggregates in the cytoplasm. Numerous mutations in the gene encoding TDP-43 have also been linked to familial cases of ALS (fALS) and cause TDP-43 proteinopathy. This study attempts to decipher how the molecular chaperone Hsp90 and its co-chaperones, Aha1, Sti1, and Cdc37, modulate TDP-43 aggregation, mislocalization, and toxicity using a yeast model and cultured mammalian cells. We propose that Hsp90 stabilizes aberrant forms of TDP-43 and the inhibition of Hsp90 through moderate overexpression of Sti1 is able to rescue TDP-43 toxicity by modifying cytoplasmic TDP-43 aggregates.

Keywords

Acknowledgments

First of all, I would like to thank ALS Canada for their generous support that made this study possible. I would also like to thank our collaborators Dr. Aaron Gitler (Stanford University), Dr. Marco Prado (Western University), and Dr. Michael Strong (Western University) for courteously providing us with the materials necessary for this study.

It has been a great honor working with everyone from the Duennwald Lab, and I'm especially grateful to Dr. Martin Duennwald for all the opportunities he has given. I have learnt so much under your supervision. I am also thankful of members of the Duennwald Lab, Vy and Sonja, for creating an awesome lab environment, our undergrad Soojie for helping me with my project, Anne for tirelessly answering my questions, and Alex for his tips on thesis writing.

I would also like to thank the members of my advisory committee, Dr. Christopher Howlett, Dr. Zia Khan, and Dr. Patrick Lajoie for providing me with valuable feedback on my project and guiding me through my master's program at Western.

Finally, I would like to thank my family—my parents and Scott. Thank you for your support, I wouldn't have been able to do it without you.

Table of Contents

List of Tables

List of Figures

List of Appendices

List of Abbreviations

2xYT	2x yeast extract tryptone
AD	Alzheimer's disease
Aha1	Activator of Hsp90 ATPase protein 1
ALS	Amytrophic lateral sclerosis
Amp	Ampicillin
AZC	azetidine-2-carboxylic acid
BCA assay	Bicinchoninic acid assay
BSA	Bovine serum albumin
Cdc37	Cell Division Cycle protein 37
DMSO	Dimethyl sulfoxide
DNA	Deoxyribonucleic acid
dNTP	Deoxynucleotide
ER	Endoplasmic reticulum
fALS	Familial ALS
FTD	Frontaltemporal dementia
FBS	Fetal Bovine Serum
Gal	Galactose
GFP	Green fluorescent protein
HD	Huntington's disease
HIV	Human immunodeficiency virus
HSF	Heat Shock Factor
Hsp	Heat shock protein
Kan	Kanamycin
LB	Lysogeny Broth

Li	Lithium
MAT	Mating type
MG132	Carbobenzoxy-L-leucyl-L-leucyl-L-leucinal
mRNA	Messenger RNA
NEM	N-Ethylmaleimide
NES	Nuclear export sequence
NLS	Nuclear localization sequence
OD_{600}	Optical Density at 600 nm
PBST	Phosphate buffered saline with tween
PCR	Polymerase chain reaction
PD	Parkinson's disease
PEG	Polyethylene glycol
PGK-1	Phosphoglycerate Kinase 1
PMSF	Phenylmethylsulfonyl fluoride
polyQ	poluglutamine
RNA	Riboneucleic acid
ROS	Reactive oxygen species
RRM	RNA recognition motif
sALS	Sporadic ALS
SD	Selective dextrose
SDD-AGE	Semi-Denaturating Detergent Agarose Gel Electrophoresis.
SDS	Sodium dodecyl sulfate
SDS-PAGE	Sodium dodecyl sulfate polyacrylamide gel electrophoresis
SGal	Selective galactose
SOD1	Superoxide dismutase 1
Sti1	Stress inducible protein 1

TDP-43	Transactive Response DNA-binding protein 43
TPR	Tetratricopeptide repeat
TE	Tris-EDTA
UPS	Ubiquitin proteasome system
v/v	Volume/volume
WT	Wild type
YFP	Yellow fluorescent protein
YPD	Yeast extract peptone dextrose

Chapter 1

1   Introduction

Neurodegenerative diseases, such as Alzheimer's Disease (AD), Parkinson's Disease (PD), Huntington's Disease (HD), and amyotrophic lateral sclerosis (ALS), are characterized by the progressive loss of function and death of neurons leading to dementia and ultimately the death of patients. They are also associated with misfolding and aggregation of disease proteins. In ALS, the accumulation of the TAR DNA-binding protein (TDP-43) in pathological neuronal inclusions of patient's brain and spinal cord is found in the vast majority of patients. These pathological inclusions are a result of the mislocalization of TDP-43 from the nucleus and the formation of aggregates in the cytoplasm. This phenomenon is known as TDP-43 proteinopathy, and observed in about 97% of all ALS patients [1].

It is essential for proteins to obtain and maintain their proper native conformations to perform their biological functions. Yet proteins can misfold or aggregate due to genetic mutations, avert environmental factors, and aging. Consequently, cells have evolved several mechanisms to defend against protein misfolding and aggregation [2]. Once proteins misfold and aggregate, they fail to obtain their proper conformations and cannot perform their regular cellular functions, i.e. toxicity associated with loss of function. Misfolded proteins can also disturb regular cellular physiology and thus become toxic, i.e. toxicity associated with gain of function. Through mechanisms, such as protein remodeling by molecular chaperones or degradation by the ubiquitin proteasome pathway and autophagy [2], cells ensure proper protein quality and normal function of all biological processes. My study focuses on how cellular protein quality control regulates TDP-43 misfolding via the action of molecular chaperones.

Molecular chaperones guide misfolded proteins to refold into their native conformations, thus reducing toxicity and restoring regular function. Many molecular chaperones are induced in response to stressful conditions, including heat and chemical stress, as proteins have a tendency to misfold under stressful conditions. Molecular chaperones bind to

partially folded or exposed hydrophobic regions of proteins in order to stabilize them and prevent further misfolding and aggregation. Proteins are released after chaperones have successfully refolded them into their functional conformation [3]. In addition, chaperones have also been reported to prevent the aggregation of unfolded polypeptide chains, cooperate with proteases to facilitate protein degredation, as well as act as disaggregases, i.e. directly dissolving protein aggregates [4]. More recently, molecular chaperones have also been shown to ameliorate the toxic effects of protein misfolding and aggregation [5]. My studies focus on the role of the molecular chaperone Hsp90 and its co-chaperones in the regulation of TDP-43 misfolding and the associated toxicity.

Hsp90 plays central roles in key cellular pathways, such as cellular signaling, cell cycle control, cell survival, as well as guiding structural formation of proteins [6]. Data from a genome-wide yeast study indicate that Hsp90 is required for 10% of all proteins to function properly, whether by direct interactions or indirect interactions mediated by co-chaperones [7]. Hsp90 functions with the aid of its co-chaperones that regulate Hsp90 activity and its specific binding to client proteins [8].

My research focuses on the highly conserved Hsp90 co-chaperones Aha1, Cdc37, and Sti1. Aha1 stimulates Hsp90 ATPase activity and is a potent activator of its activity, whereas both Cdc37 and Sti1 inhibit Hsp90 ATPase activity [8]. Targeting Hsp90 and its co-chaperones as a potential therapeutic approach to treat neurodegenerative diseases has been thoroughly studied in recent years [9]. Despite the beneficial role of Hsp90 in many cellular processes, it has been suggested that Hsp90 allows toxic aberrant protein aggregates to accumulate by maintaining their stability under non-physiological conditions [10]. Thus, inhibition of Hsp90 may prove to be a viable therapeutic approach to treat neurodegenerative diseases, as it activates the heat shock factor (HSF-1) and in turn promotes the expression of other neuroprotective chaperones that are responsible for protein disaggregation and degradation [9].

In studies on tau aggregation, observed in Alzheimer's disease and other tauopathies, Hsp90 co-chaperones have been shown to control whether tau aggregates are toxic or benign by specific interaction with co-chaperones [4]. This co-chaperone mediated

alteration of tau aggregation suggests that the activity of Hsp90 and its co-chaperones are important in regulating protein misfolding and toxicity in neurodegenerative disease beyond tauopathies. Of note, Hsp90 levels are relatively high and static in the aging brain whereas co-chaperone expression is more dynamic [4].

My study aims to understand how Hsp90 and its co-chaperones modulate the toxicity of TDP-43 using a yeast model and cultured mammalian cells. The benefits of using yeast models to investigate TDP-43 toxicity are well established as they recapitulate many central aspects of ALS pathology, including TDP-43 toxicity, aggregation, and mislocalization [11]. Yeast orthologues of Hsp90 and its co-chaperones are also well described [12]; in fact, many functional and structural features of Hsp90 and its co-chaperones were initially established by studies in yeast. Our vast knowledge of the yeast genome and proteome as well as the plethora of available research tools, such as genome-wide deletion and overexpression libraries, make yeast an optimal experimental system to study how Hsp90 and its co-chaperones modulate TDP-43 misfolding and toxicity [13].

1.1   Protein Quality Control

Proteins are essential components to maintaining cellular homeostasis and are responsible for many cellular processes. The function of proteins is not only determined by its amino acid sequences, but also by the proper three-dimensional folding of its polypeptide chains. The folding of proteins into their native conformation is vital for them to perform their biological functions. Though the native conformation of a protein is thermodynamically favored in the equilibrium between partially folded or misfolded states and the native state (Figure 1) [14], proteins have an intrinsic tendency to misfold or aggregate [15], as stable interactions of partially folded intermediate proteins can occur to promote misfolding and aggregation [16]. The balance between the native state of a protein and other non-native states is delicate. As a consequence, cells have developed several mechanisms to combat protein misfolding and aggregation, known as cellular protein quality control.

Misfolded Partially Folded Native State
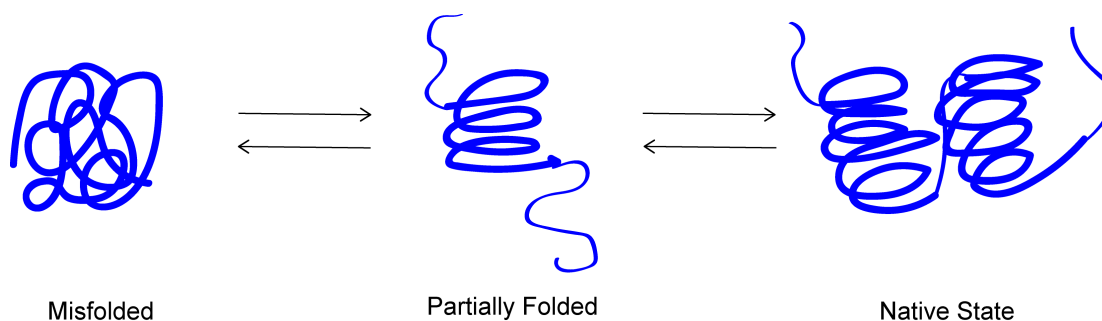
Figure 1: Equilibrium between the native state of a protein and other non-native species. Though the native state of a protein is most stable thermodynamically, proteins are constantly being unfolded and misfolded in the cell and rely on protein quality control mechanisms to rectify its conformation.

Cellular protein quality control aims to maintain protein homeostasis, or proteostasis, in the cell through regulating the accurate production, folding of all proteins, and the refolding or degradation of misfolded proteins, or through sequestering misfolded proteins to specific quality control compartments [14]. Molecular chaperones are central to cellular protein quality control as they determine whether a misfolded protein should be refolded, degraded through the ubiquitin proteasome system (UPS) or autophagy, or sequestered into cellular quality control compartment to minimize toxicity [14]. The role and function of specific molecular chaperones will be discussed in more detail in the following section.

It has become increasingly evident through recent research that the accumulation of protein misfolding and aggregation is the hallmark of an expanding list of "protein-conformational diseases" [17], including lysosomal storage disease, cystic fibrosis, cancer, and neurodegenerative disease [14]. Although the mechanisms by which proteins misfold remains unclear, it is evident that environmental and metabolic stresses and aging are major factors that contribute to increased protein misfolding [14]. These stress conditions increase the burden on the cellular protein quality control machinery to maintain proteostasis often beyond its capacity, leading or contributing to disease [18].

1.2   Molecular Chaperones

Molecular chaperones are central to cellular protein homeostasis. Their role in protein quality control ranges from protein maturation by guiding the folding of newly synthesized proteins to the refolding of misfolded proteins [16]. In addition to refolding of misfolded proteins, they can also prevent the aggregation of the unfolded polypeptide chains of misfolded or exposed proteins and act as a disaggregases to pull apart aggregates [4]. Recent studies have also shown that chaperones suppress cytotoxicity associated with protein aggregation [4]. Molecular chaperones are also responsible for determining whether a protein should be folded back to its native conformation or degraded by the UPS or autophagy [4, 17]. Lastly, they also direct potentially toxic protein species to be sequestered into cellular compartments and "quarantined" [14] (Figure 2). Chaperones perform all these functions through cycles of substrate binding and release that is often ATP-dependent. Although most chaperones are able to bind to substrates independently, many of them rely on co-chaperones to modulate efficiency and specificity [19]. Co-chaperones play key roles in the molecular chaperone machinery, including regulation of ATPase activity, determining the specificity of chaperone substrates, and directing substrates to be either refolded or degraded.
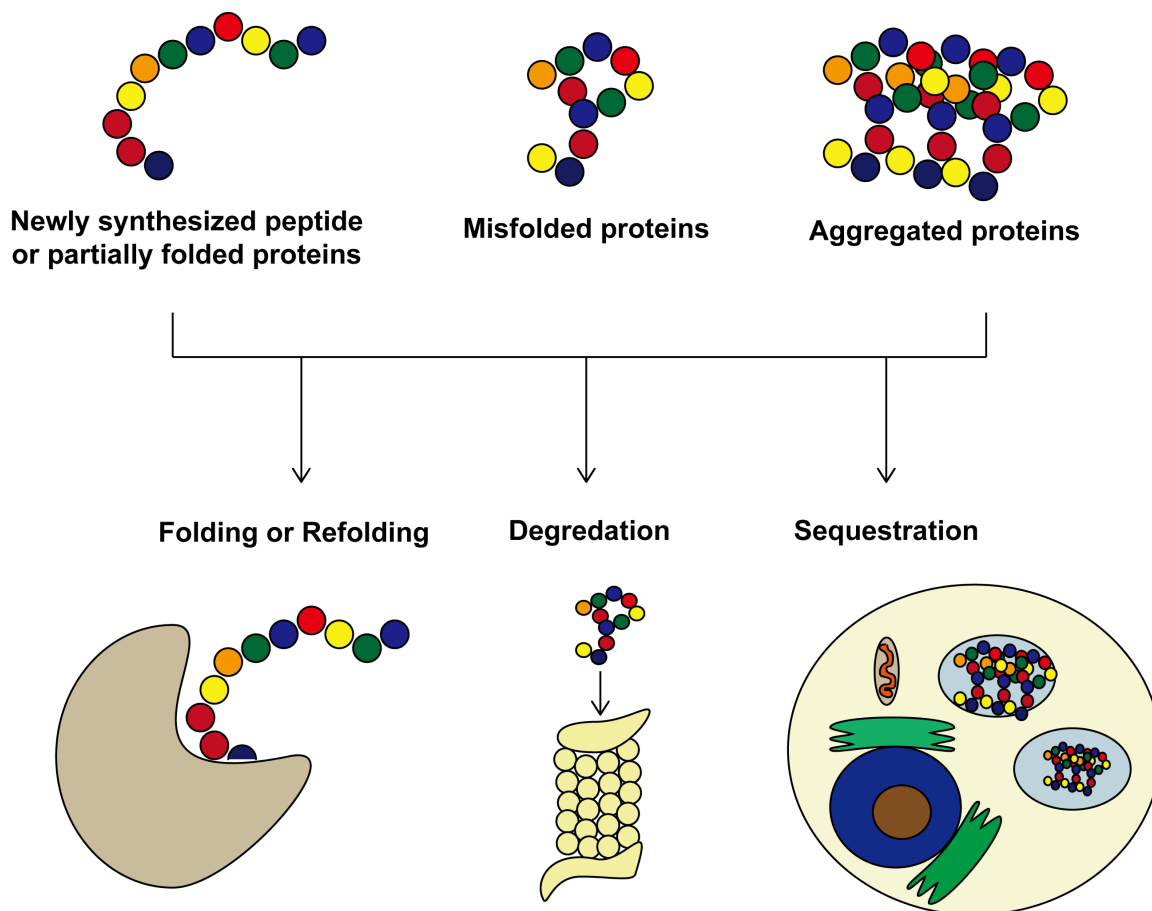
Figure 2: The role of molecular chaperones in maintaining proteostasis. Molecular chaperones are responsible for folding newly synthesized peptides or assist in refolding misfolded protein into their native conformation. If the protein species cannot be refolded back into their native conformation, they are sent to be degraded through the UPS or autophagy. Molecular chaperones can also sequester toxic protein species into cellular compartments to be "quarantined". (Adapted from Chen, Retzlaff et al. 2011 [14])

The heat shock response is activated when cells encounter stressful conditions such as environmental stress, chemical stress, heat stress, and pathological stresses that can ultimately lead to denaturing and misfolding of proteins. The key player induced by the heat shock response is a group of molecular chaperones named "heat shock proteins" (Hsps). Heat shock proteins are ubiquitously expressed and classified into gene families, according to their molecular weight: Hsp110, Hsp90, Hsp70, Hsp60, Hsp40, and small Hsps (sHsp) [19]. In this study, we mainly focus on Hsp90 and its co-chaperones.

1.2.1 Hsp90

Hsp90 is a highly conserved cytosolic molecular chaperone that plays central roles in key cellular pathways, such as cellular signaling, cell cycle control, cell survival, as well as guiding structural formation of proteins [6]. It is responsible for the folding activation of over 200 different client proteins [20]. The structure of Hsp90 consists of an N-terminus responsible for ATP binding, a middle domain responsible for substrate and co-chaperone binding, and a C-terminus that is essential for dimerization of the protein (Figure 3A and D) [21]. In eukaryotes, a MEEVD polypeptide chain is attached to the C-terminus of Hsp90, responsible for binding to co-chaperones with tetratricopeptide repeats (TPR) [22]. Dimerization is essential to Hsp90 function in vivo [23] and contributes to the open and closed conformation of Hsp90's ATPase cycle (Figure 3B). The dimerization of Hsp90 results in a "clamp" like structure that maximizes binding with client proteins; once the N-terminus binds to ATP, Hsp90 adopts a "closed" conformation that allows for interaction with client protein, in addition to ATP hydrolysis [24]. The chaperoning ability of Hsp90 is strongly dependent on the binding and hydrolysis of ATP and essential for the function of Hsp90 in vivo [25]. Although Hsp90 function is dependent on ATPase activity, ATP turnover is very slow and requires mediation by a large group of molecular co-chaperones to influence its ATPase cycle by inhibiting or stimulating its ATPase activity and change its conformation [21, 26].

There are two forms of Hsp90, Hsc82 and Hsp82, in yeast and in most other eukaryotic systems. Hsc82 is constitutively expressed at high levels, whereas Hsp82 is normally expressed at much lower levels and strongly induced under stress conditions. The two proteins share ~97% sequence homology and are functionally redundant. Only one

isoform needs to be present in the cell for viability under normal temperatures [7]. At higher temperatures, both isoforms are expressed at high levels, providing a buffer for the fluctuation in protein folding efficiency.

Hsp90 has been thoroughly studied in recent years [9] as a potential therapeutic target for neurodegenerative diseases, as Hsp90 has been found to co-localize with aggregates of disease related proteins, such as amyloid Beta (Aβ) plaques and tau in Alzheimer's disease (AD) [4]. Though Hsp90 has been reported to reduce the aggregation-propensity of numerous proteins such as Aβ [27, 28], recent studies suggest that inhibition of Hsp90 and the ensuing induction of the heat shock response may be beneficial in other neurodegenerative diseases and thus has the potential of becoming a therapeutic target [9]. Also, it is speculated that Hsp90 can stabilize toxic protein species through binding and contribute to disease progression [9]. Inhibition of Hsp90 can therefore direct toxic protein species to be degraded through the UPS (Figure 3C) [29]. Collectively, these studies provide a strong rationale to further explore the role of Hsp90 in protein misfolding in neurodegenerative diseases.
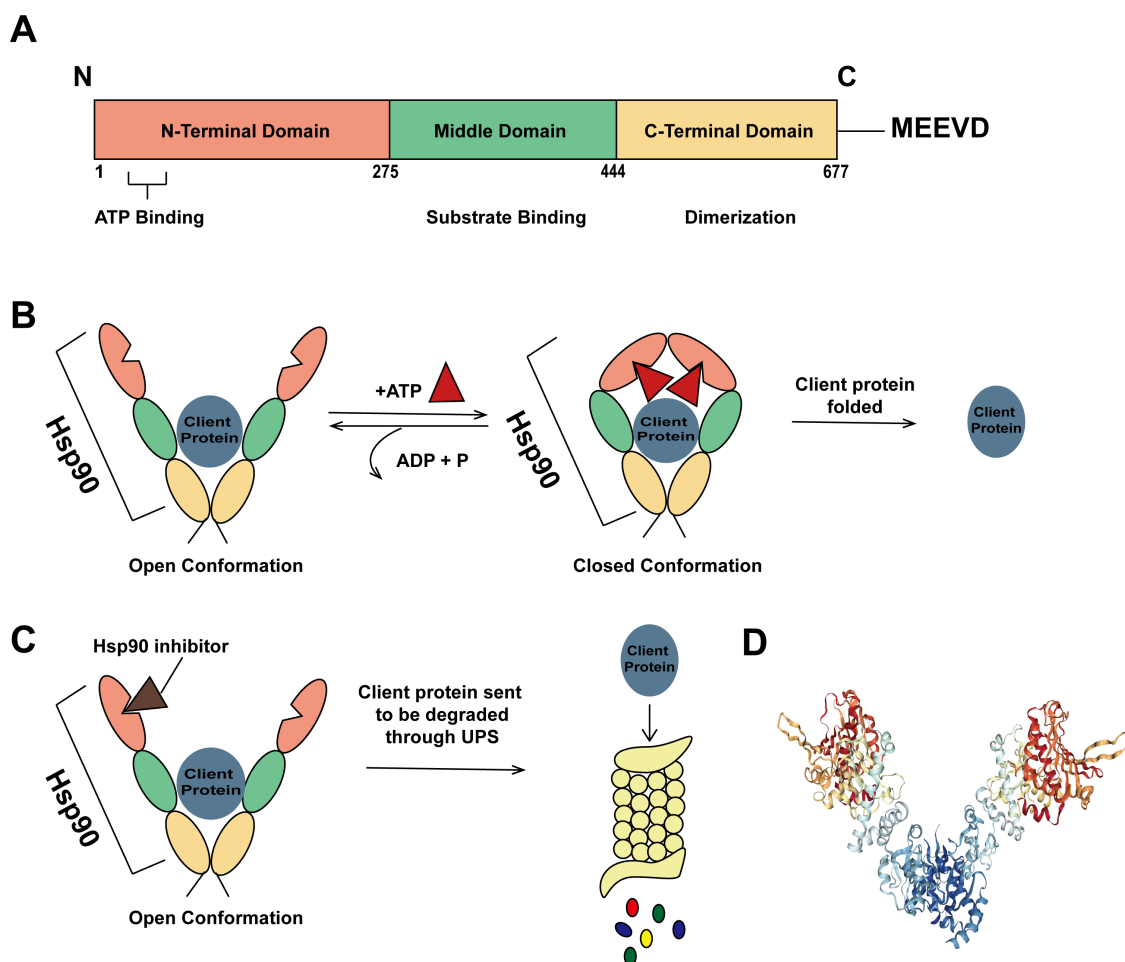
Figure 3: Structure of Hsp90 and its interaction with client proteins. **A** Structural schematic of yeast heat-inducible Hsp90 with its three domains, the N-terminal domain, the middle domain, and the C-terminal domain. **B** ATP-dependent mechanism of Hsp90-client protein binding, ATP binds to the N-terminal ATP binding domain, inducing the Hsp90 closed conformation for maximal substrate binding. **C** Presence of Hsp90 inhibitors prevents ATP-binding and the closed conformation, the client protein is sent to be degraded through UPS instead. **D** Crystal structure of the E. coli Hsp90 dimer (PDB ID 2IOQ [30]) (Adapted from Garcia-Carbonero, Carnero et al. 2013 [29] and Terasawa, Minami et al. 2005 [22])

1.2.2   Hsp90 Co-chaperones

Hsp90 function relies heavily on the binding and hydrolysis of ATP and the specific binding to client proteins, which can be achieved through the cooperation with various co-chaperones. Co-chaperones are able to inhibit or stimulate the ATPase activity of Hsp90 and facilitate the folding or activation of its client proteins [26]. In this study, we focus on the Hsp90 co-chaperones Aha1, Cdc37, and Sti1.

1.2.2.1   Aha1

Aha1 (activator of Hsp90 ATPase) was first identified in yeast as a stress-regulated protein that interacts directly with Hsp90 to stimulate its ATPase activity along with its shorter homologue, Hch1. [25]. It was later found to bind to the middle domain of Hsp90 and to stimulate its ATPase activity by up to twelve fold over its basal level [25, 31]. Aha1 is also involved in the activation of client proteins such as tyrosine-protein kinase transforming protein (v-Src) and the glucocorticoid receptor (GR) [32].

Aha1 is a cytoplasmic protein that is highly conserved in eukaryotes. It is divided into two domains: the N-terminal domain and the C-terminal domain. Both of these domains are required for interaction with Hsp90 (Figure 4A and C) [33]. Aha1 first interacts with Hsp90 through the asymmetric binding of its N-terminus to the M-domain of Hsp90 (Figure 4B). The C-terminus of Aha1 is capable of binding to the N-terminal ATP-binding domain of Hsp90 to induce its closed conformation and facilitate ATP binding and hydrolysis [33]. The binding of Hsp90 and Aha1 is independent of ATP at the N-terminal domain of Hsp90 [26].

Aha1 has also been found to act independently of Hsp90 and interact with stress-denatured proteins to prevent their aggregation [34]. This suggests that Aha1 may play an important role in protein folding under stress conditions by directing misfolded proteins to be degraded through ubiquitin-dependent pathways.
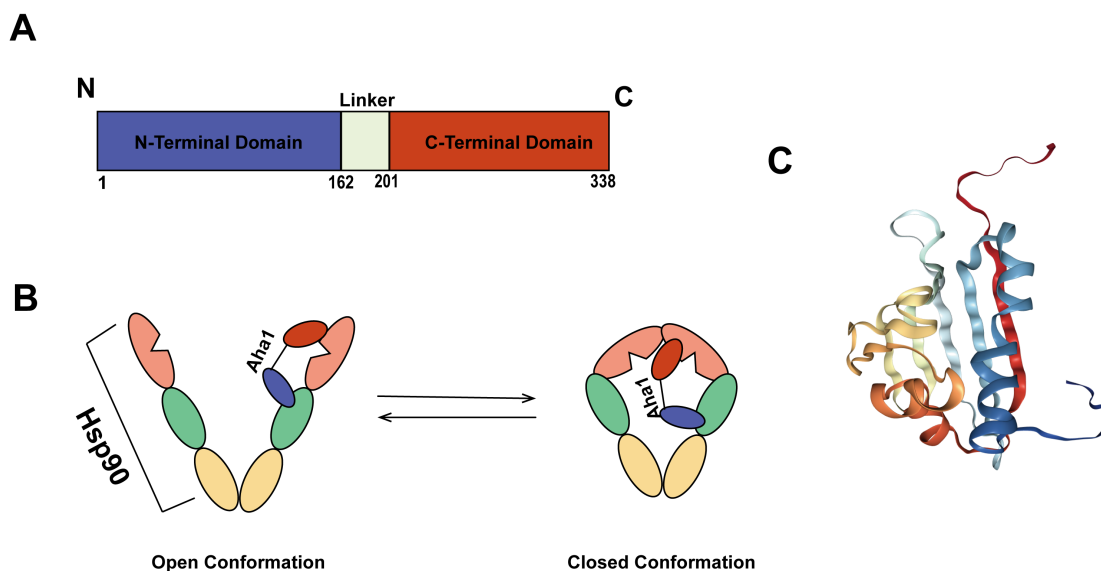
Figure 4: Structure of Aha1 and its interaction with Hsp90. A Structural schematic of Aha1 consisting of two domains, the N-terminal domain and the C-terminal domain connected by a linker. **B** Aha1 binds asymmetrically to Hsp90 by binding to the middle domain of Hsp90 through its N-terminal domain, and the N-terminal domain of Hsp90 through its C-terminal domain to stimulate the ATPase activity of Hsp90 and induce its closed conformation. **C** Crystal structure of human Aha1 (PDB ID 1X53 [35])

1.2.2.2   Cdc37

Cdc37 (Figure 5A and C), also known as p50, was first discovered in a screen for genes related to the c̲ell d̲ivision c̲ycle in yeast [36], and it is essential to drive cell proliferation [37]. It is conserved from yeast to humans, though homologues to Cdc37 have yet to be found in plants [38]. It plays an essential role in stabilizing and stimulating the activity of protein kinases [38]. The binding of the C-terminal domain of Cdc37 to the ATP-binding domain of Hsp90 inhibits the ATPase activity of Hsp90 and it is thought to prolong interactions between client proteins and Hsp90 in order to facilitate more effective chaperoning activity (Figure 5B) [38, 39].

In addition to its role as a co-chaperone of Hsp90, Cdc37 is able to function independently as a molecular chaperone with strikingly similar activities to Hsp90 and

can even compensate for decreased Hsp90 function in vivo [40]. The Cdc37-Hsp90 complex has also been found to influence protein quality control through activation of autophagy [38]. The involvement of the Cdc37-Hsp90 complex in autophagy may be important in neurodegenerative diseases, as it may play a role in the clearance of the accumulation of aggregates in these diseases [38].

A

B
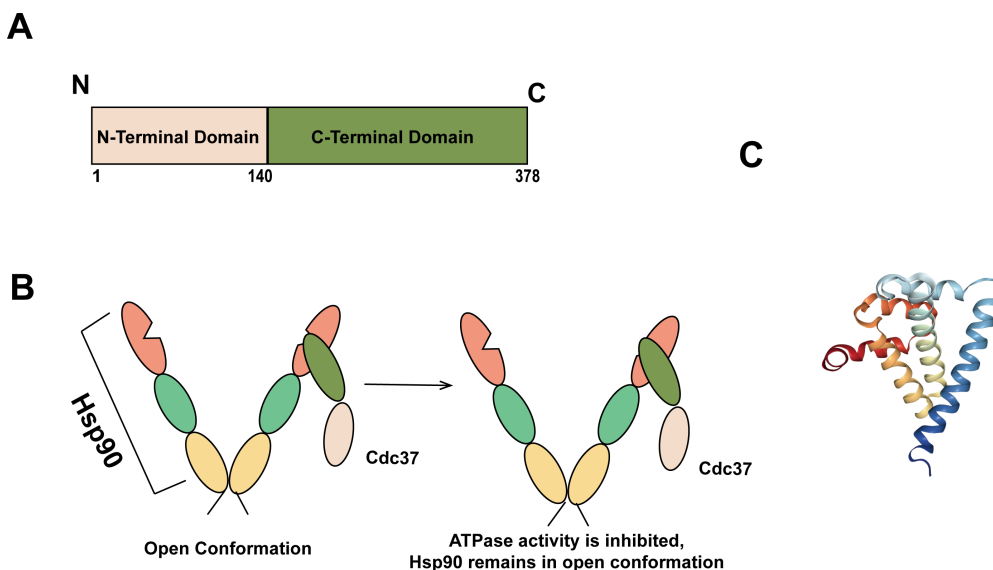
Figure 5: Structure of Cdc37 and its interaction with Hsp90. A Structural schematic of Cdc37 consisting of two domains, the N-terminal domain and the C-terminal domain. **B** Cdc37 binds asymmetrically to Hsp90 by binding to the ATP-binding domain of Hsp90 through its C-terminal domain, thus inhibiting its ATPase activity. **C** Crystal structure of human Cdc37 (PDB ID: AW0G [41]).

1.2.2.3 Sti1

Sti1 (Stress-inducible protein 1), also known as Hop (Hsp70/Hsp90 Organizing Protein) in animals, was first identified in yeast as a trans-acting factor that induces heat-shock gene expression [42]. Sti1 homologues have since been identified in many different organisms and can generally be divided into yeast Sti1 (ySti1), plant Sti1, and animal Sti1 (Hop) [43]. The structure of Sti1 is shown in Figure 6A and D. Sti1 contains nine tetratricopeptide repeat (TPR) motifs that are clustered into three domains with three TPR

motifs per domain. The TPR domains are important for directing protein-protein interactions. Sti1 is capable of binding to the MEEVD polypeptide chain of Hsp90 and the PTIEVVD polypeptide chain of Hsp70 simultaneously through its TPR motifs to connect Hsp90 to Hsp70 [22].

The binding of Sti1 to Hsp90 inhibits Hsp90's ATPase activity and stabilizes the open conformation of Hsp90, which allows unloading of the client protein from Hsp70 into the open "clasp" of Hsp90 once Sti1 also binds to the Hsp70-client protein complex (Figure 6B) [22]. After the client protein binds to the middle domain of Hsp90, Aha1 out-competes Sti1 to stimulate the ATPase activity of Hsp90 to change the conformation of Hsp90 from open to closed (Figure 6C) [32].

Sti1 is largely cytoplasmic under normal conditions, though nuclear-localization of the protein has also been observed in small quantities [43]. Sti1 also has a nuclear localization sequence (NLS) overlapping with its Hsp90-binding TPR2A domain, suggesting an alternate binding of Sti1 to Hsp90 and various nuclear import factors to retain Sti1 in either the cytoplasm or the nucleus, respectively [43].

In addition to function as a Hsp90 co-chaperone, Sti1 partakes in other cellular processes independently of Hsp90. Notably, Sti1 is involved in protein folding through the Cdc37 chaperone complex and the prion protein complexes, which are responsible for the folding of protein kinases and recruiting and curing of prions, respectively [43]. In yeast, overexpression of Sti1 has been shown to interfere with the propagation and manifestation of prions and consequently suppression of the expression of prion proteins [44]. This leads to the speculation that Sti1 cures prions by inhibiting the formation of non-soluble aggregates of prion protein or prevents its structural conversion from the cellular form to the scrapie form [43]. We focus on Sti1 in this study due to its various roles in protein folding and aggregation.
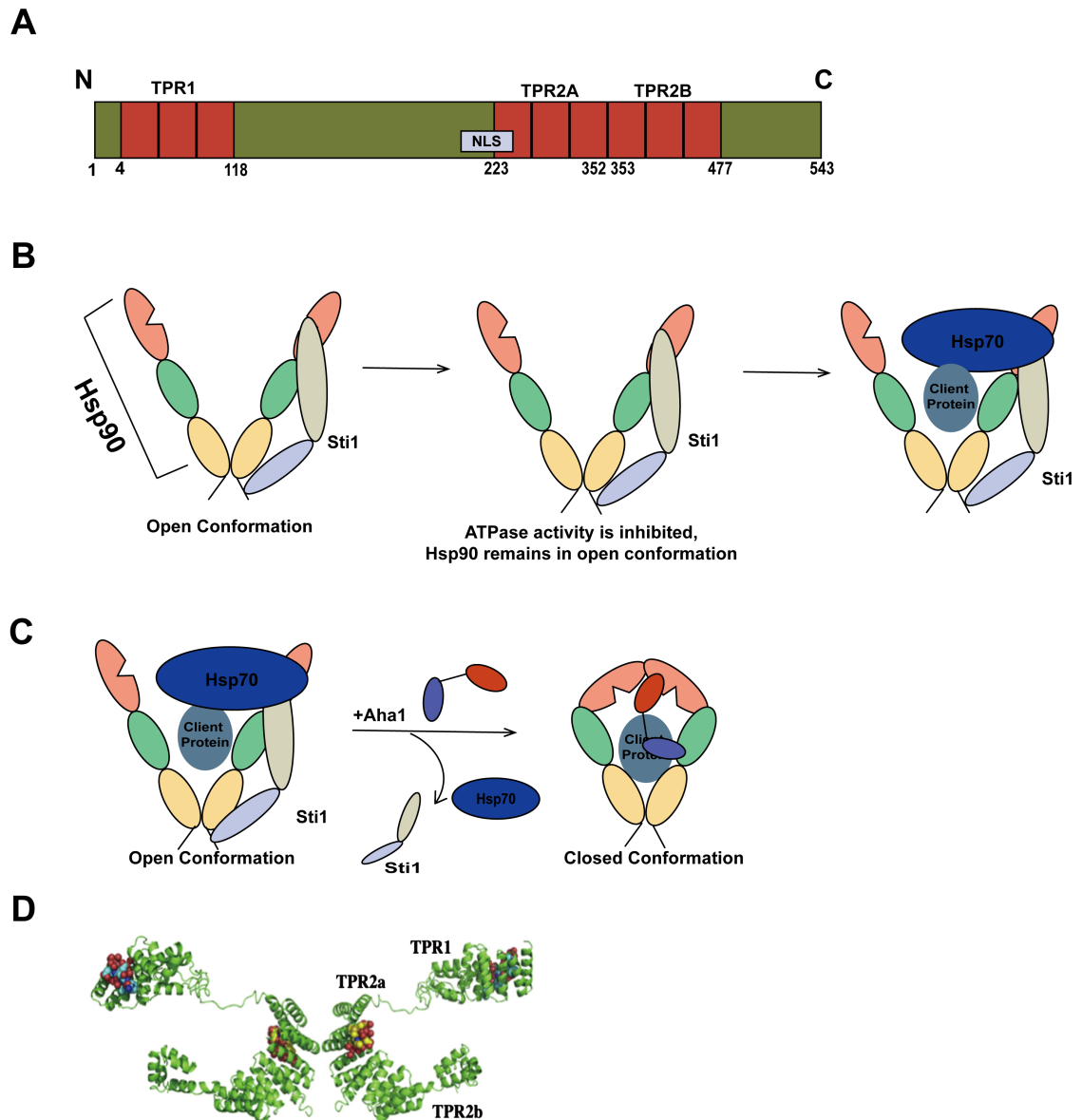
Figure 6: Structure of Sti1 and its interaction with Hsp90. **A** Structural schematic of Sti1 consisting of three tetratricopeptide repeat (TPR) domains with three TPR motifs each and a nuclear localization sequence (NLS). **B** Sti1 binds to the C-terminal MEEVD peptide and the ATP-binding domain of Hsp90 through its TPR domains to link the Hsp70-client protein complex with Hsp90 and transfer the client protein from Hsp70 to Hsp90. **C** Aha1 outcompetes Sti1 to bind to the ATP-binding domain of Hsp90 and induces the closed conformation of Hsp90. **D** Model structure of Sti1, the TPR1 and TPR2a domains are shown bound with Hsp70 and Hsp90 (Picture from Prodromou, 2012 [45]. (Adapted from Odunuga et al. [43] and Li et al. [20])

1.3   Neurodegenerative Disease

Protein misfolding and aggregation is the central hallmark of many neurodegenerative diseases such as Alzheimer's Disease (AD), Huntington's Disease (HD), Parkinson's Disease (PD), amyotrophic lateral sclerosis (ALS), and frontotemporal dementia (FTD).

The prominence of protein misfolding and aggregation in neurodegenerative disease can perhaps be explained by the fact that neurons are particularly susceptible to stress conditions including genetic and environmental changes to cellular proteostasis [4]. In addition, aging is a factor that contributes to the decline of the cell's capacity to maintain proteostasis as old cells accumulate mutations and damaged proteins that can overwhelm the overall balance of cellular proteostasis [14]. This line of thinking is consistent with the late, age-dependent onset of most neurodegenerative diseases.

In order to combat the accumulation of damaged or misfolded proteins in the aging cell, particular chaperones are up-regulated to prevent aggregation and facilitate their refolding or degradation [46]. Though molecular chaperones show altered or even impaired induction in the aging cell, the expression level of heat shock factor-1 (HSF-1), the transcription factor responsible for the induction of most of the genes encoding chaperones, stays surprisingly unchanged [46]. Yet the binding of HSF-1 to the heat shock element leading to the activation of HSF-1 decreases in aging cells, which in turn does not activate the heat shock response properly [46].

Hsp90 has been found to repress HSF-1 activity. It is proposed that under normal conditions, Hsp90 and HSF-1 forms a complex that inhibits the activities of HSF-1; however, under heat shock conditions, HSF-1 is released from the Hsp90-complex activates the heat shock response [47]. Since the inhibition of Hsp90 has been reported to stimulate HSF-1 activation [48], it was proposed that in the case of neurodegenerative diseases with characteristic protein aggregates, the inhibition of Hsp90 can activate HSF-1 and lead to increased induction of other chaperones such as Hsp70 and Hsp40 that can aid in protein disaggregation and degradation [9]. Furthermore, inhibition of Hsp90 can prove to be beneficial in protein misfolding diseases, as it is speculated that Hsp90

stabilizes misfolded or aberrant protein species that can lead to an accumulation in toxic aggregates [9].

1.4   Amyotrophic Lateral Sclerosis (ALS)

Approximately two in 100,000 people develop Amyotrophic Lateral Sclerosis (ALS) [49]. ALS, also known as Lou Gehrig's disease, is a neurodegenerative disease characterized by progressive impairment of muscle function due to neuronal loss often leading to fatal paralysis of the respiratory system. The disease has an onset average age of ~60 years and is fatal within 3-5 years following disease onset [50]. The only treatment currently available for ALS is Riluzole; yet the drug is not at all an effective treatment as it only extends the lifespan of patients for about three months [51]. ALS can be divided into two forms, sporadic ALS (sALS) and familial ALS (fALS). sALS accounts for up to 95% of all ALS cases, whereas fALS only accounts for about 5% [52].

The first cause for fALS was identified in 1993 as a mutation in the copper-zinc superoxide dismutase 1 (SOD1) gene [53]. Mutations in the gene are responsible for about 20% of fALS cases and 1% of sALS [51]. SOD1 is an enzyme that converts superoxide anions into hydrogen peroxide and oxygen, thus reducing the levels of free radicals and reactive oxygen species (ROS) and protecting cells from oxidative stress. The mechanism by which mutations in SOD1 contribute to ALS pathogenesis remains unclear. Since mutant SOD1 shows no decrease in free-radical scavenging and copper binding abilities [54], it has been speculated that rather than loss-of function in mutant SOD1, a gain-of-function mechanism is responsible for ALS disease progression through the formation of aggregates. Studies have also found mutant human SOD1 (hSOD1) to destabilize native SOD1 and lead to the formation of misfolded aggregates and degradation of SOD1 [54]. Furthermore, mutant SOD1 has been found to seed misfolding of wild type (wt) SOD1, allowing the aggregation of wt SOD1 and the propagation of SOD1 misolding in a prion-like manner [55, 56].

SOD1 remained the only known ALS protein until the recent discovery of the TAR DNA Binding protein (TDP-43) inclusion bodies in brains of ALS patients in 2006 [57]. Also, TDP-43 mutations account for ~5% of fALS and ~1% of sALS [58]. Following the

discovery of TDP-43 as a cause for ALS, other genetic mutations have been linked to fALS, such as mutations in Fused in Sarcoma (FUS) in 2009 [59], C9ORF72 in 2011 [60], Rho guanine nucleotide exchange factor (RGNEF) [61], and the more recent discovery of NEK-1 in 2016 [62]. C9ORF72 mutations account for about 40-50% of all fALS cases and up to 20% of sALS cases, making it the most prominent genetic cause for ALS found so far [58].

At a pathological level, ALS is characterized by protein aggregates or inclusions in motor neurons containing FUS, TDP-43, RGNEF, SOD1, neurofilaments (NF), ubiquitin, peripherin, and others [63]. Though in the vast majority (95%) of all ALS cases, TDP-43 proteinopathy is observed (Figure 7) [64]. In TDP-43 proteinopathy mutant or wild type TDP-43 is mislocalized from the nucleus to the cytoplasm followed by the formation of ubiquitinated inclusions or aggregates in the cytoplasm of neurons and occasionally glia cells of patient's brain [65]. TDP-43 has also been found to co-localize with other ALS-linked proteins such as RGNEF [61], while FUS and SOD1 positive inclusion bodies are always TDP-43 negative [58]. In this study, we focus on TDP-43 proteinopathy as a cause for ALS due to its prominence in ALS patients. TDP-43 will be discussed further in the following section.

Table 1: Genetic mutations associated with ALS.

Genetic Subtype	Gene	Inheritance	Function/ Putative Function
ALS1	SOD1	AD/AR	Enzymes
ALS2	Alsin	AR	Cellular transport
ALS4	SETX	AD	RNA metabolism
ALS5	SPG11	AR	DNA damage
ALS6	FUS	AD/AR	RNA metabolism
ALS8	VAPB	AD	Cellular transport
ALS9	ANG	AD	RNA metabolism
ALS10	TARDBP	AD	RNA metabolism
ALS11	FIG4	AD	Enzymes
ALS12	OPTN	AD/AR	Protein metabolism
ALS13	ATXN2	AD	RNA metabolism
ALS14	VCP	AD	Protein metabolism
ALS15/ALSX	UBQLN2	XD	Protein metabolism
ALS16	SIGMAR1	AD	Protein metabolism
ALS17	CHMP2B	AD	Intracellular transport protein
ALS18	PFN1	AD	Axonal outgrowth
ALS19	ERBB4	AD	Enzyme
ALS20	hnRNPA1	AD	RNA metabolism
ALS21	MATR3	AD	Protein metabolism
ALS-FTD	C9ORF72	AD	RNA metabolism
NA	DCTN1	AD	Intracellular transport protein
NA	ARHGEF28	Unknown	RNA metabolism
NA	NEK-1	Unknown	DNA damage

*Abbreviations in this table: *AD* autosomal dominant, *AR* autosomal recessive, *ALS* amyotrophic lateral sclerosis, *SOD1* superoxide dismustase 1, SPG11 spastic paraplegia type 11, *SETX* senataxin, *FUS*, fused in sarcoma, *VAPB* vesicle-associated membrane protein-associated protein B, *ANG* angiogenin, *TARDBP* transactivation response DNA binding protein 43 kDa, *FIG4* factor induced gene 4, *OPTN* optineurin, *ATXN2* ataxin-2, *VCP* valosin-containing protein, *UBQLN2* ubiquilin 2, *SIGMAR1* sigma non-opioid intracellular receptor 1, *CHMP2B* chromatin modifying protein 2B, *PFN1* profilin 1, *ERBB4* erb-b2 receptor tyrosine kinase 4, *hnRNPA1* heterogeneous nuclear ribonucleoprotein A1, *MATR3*, matrin-3, *C9ORF72* chromosome 9 open reading frame 72, *DCTN1* Dynactin 1, *ARHGEF28* Rho Guanine Nucleotide Exchange Factor 28, *NEK-1* NIMA (Never In Mitosis Gene A)-Related Kinase 1.
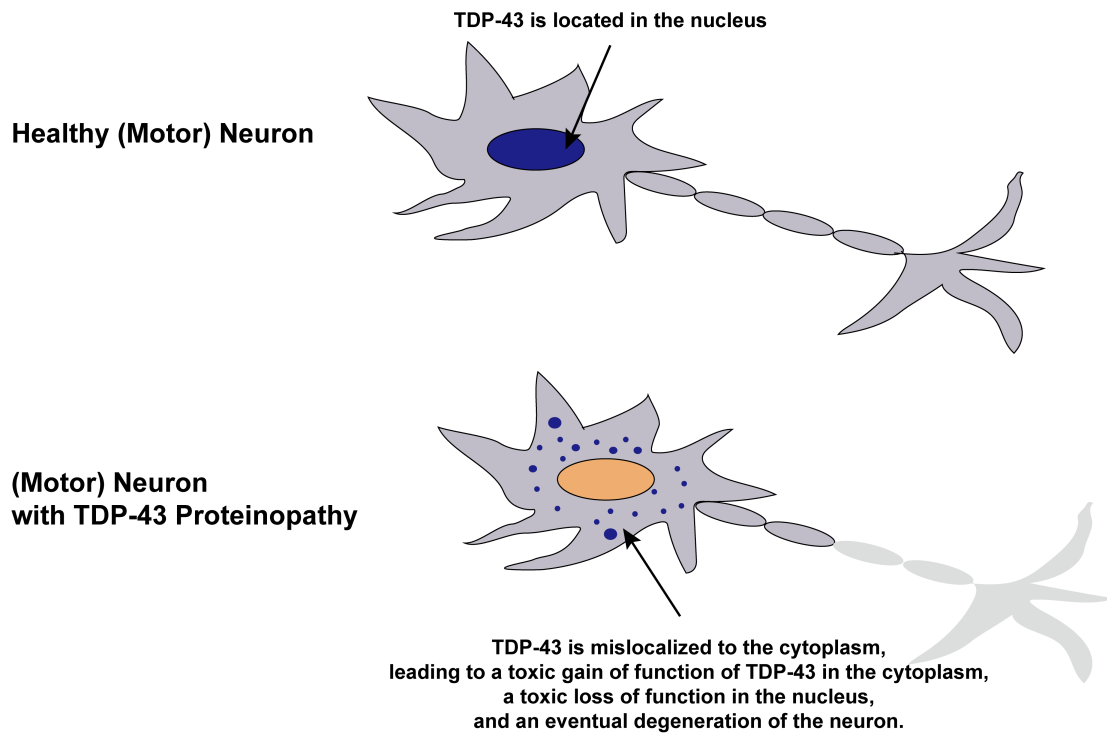
Figure 7: TDP-43 proteinopathy in neurons. In healthy neurons, TDP-43 is normally located in the nucleus. In neurons with TDP-43 proteinopathy, TDP-43 mislocalizes to the cytoplasm. The mislocalization of TDP-43 causes a toxic loss of function in the nucleus and a toxic gain of function in the cytoplasm leading to degeneration of the neuron. (Adapted from Vanden Broeck, 2014 [66])

1.5 TDP-43:
Transactive Response DNA-Binding Protein 43

Transactive Response (TAR) DNA-binding protein 43 (TDP-43), is a 43 kDa DNA/RNA-binding protein of 414 amino acids encoded by the TAR DNA-binding protein (TARDBP) gene located on chromosome 1p36.2. It is ubiquitously expressed in the nucleus of most metazoans, but constantly shuttles between the nucleus and the cytoplasm [67]. TDP-43 contains a nuclear localization sequence (NLS), two RNA recognition motifs (RRM) that are responsible for RNA binding, a nuclear export sequence (NES) located in the second RRM, and a glycine-rich prion-like domain at the C-terminus (Figure 8A) [68]. A truncation of TDP-43's C-terminus (1-216, with the NLS and NES region intact) results in both cytoplasmic and nuclear inclusion body formation, suggesting that the C-terminus plays a pivotal role in the aggregation of TDP-43 [67].

TDP-43 is involved in RNA regulation and protein production in the cell, such as regulating transcription, pre-mRNA splicing, and processing of microRNA [69], and other cellular processes such as apoptosis, cell division, and stabilization of messenger RNA [68]. Inhibition of RNA polymerase II by using actinomycin D decreases nuclear import and results in an accumulation of TDP-43 in the cytoplasm, suggesting that continuous mRNA synthesis is necessary for nuclear import of TDP-43 [67]. TDP-43 was first discovered as a protein that binds to the transactive response (TAR) DNA of the HIV-1 virus, giving its name [70] but its role in HIV-1 regulations has hence been challenged [71].

Recent studies have focused on the implication of TDP-43 in neurodegenerative diseases. TDP-43 proteinopathy is observed in the majority of ALS cases (Figure 8B) as well as the most frequent form of frontotemporal dementia (FTD), frontotemporal lobar degeneration with ubiquinated inclusions (FTLD-U) (Figure 8C). Strikingly, a portion of patients shows both FTLD and ALS features, suggesting that ALS and FTD may be a spectrum disorder (Figure 8D) [72, 73] rather than two distinct diseases. While TDP-43 was originally implicated in FTD and ALS, it has also recently been linked to Alzheimer's disease (AD) [74], Parkinson's disease (PD) [75, 76], and Huntington's disease (HD) [77]. TDP-43 proteinopathy is present in over 50% of AD patients, 60% of

PD, PD with dementia, and dementia with Lewy bodies plus AD patients, as well as co-localization of cytoplasmic inclusions with mutant huntingtin [72]. While TDP-43 inclusions are present in the majority of FLD and ALS patients, in diseases such as AD, PD, and HD, it appears to be only a secondary histopathological feature [72]. The disease form of TDP-43 is often ubiquitinated, hyperphosphorylated, or cleaved into smaller fragments of 25 and 35 kDa containing the C-terminus [78].

Fifty missense mutations in TDP-43 implicated in ALS have so far been described (Figure 8A); the vast majority of TDP-43 mutations implicated in both sporadic and familial ALS are located in the prion-like domain of the protein, with the exception of two mutations located in the N-terminus and the RRM1. This has led to the extensive studies on the prion-like domain in TDP-43 to decipher the mechanism underlying TDP-43 aggregation governed by its different domains. It has been reported that TDP-43 fragments containing the N-terminal domain and RRM1 are soluble and do not aggregate, while fragments containing RRM2 and the C-terminal region aggregated with similar efficiency as full-length TDP-43 [79], contributing to the theory that the C-terminal domain is essential for TDP-43 aggregation. It is speculated that the C-terminus is responsible for the interference of normal protein-protein interaction that can lead to impaired nuclear import of TDP-43 [68]. It has also been reported that mislocalized wild type TDP-43 can induce wild type SOD1 to misfold and aggregate [80]. These misfolded wild type SOD1 aggregates can then propagate from cell to cell to promote misfolding of SOD1 in a prion-like manner [81]. Our work focuses on how molecular chaperones interact with TDP-43 as a potential therapeutic target for TDP-43 proteinopathy in ALS and possibly other neurodegenerative diseases.
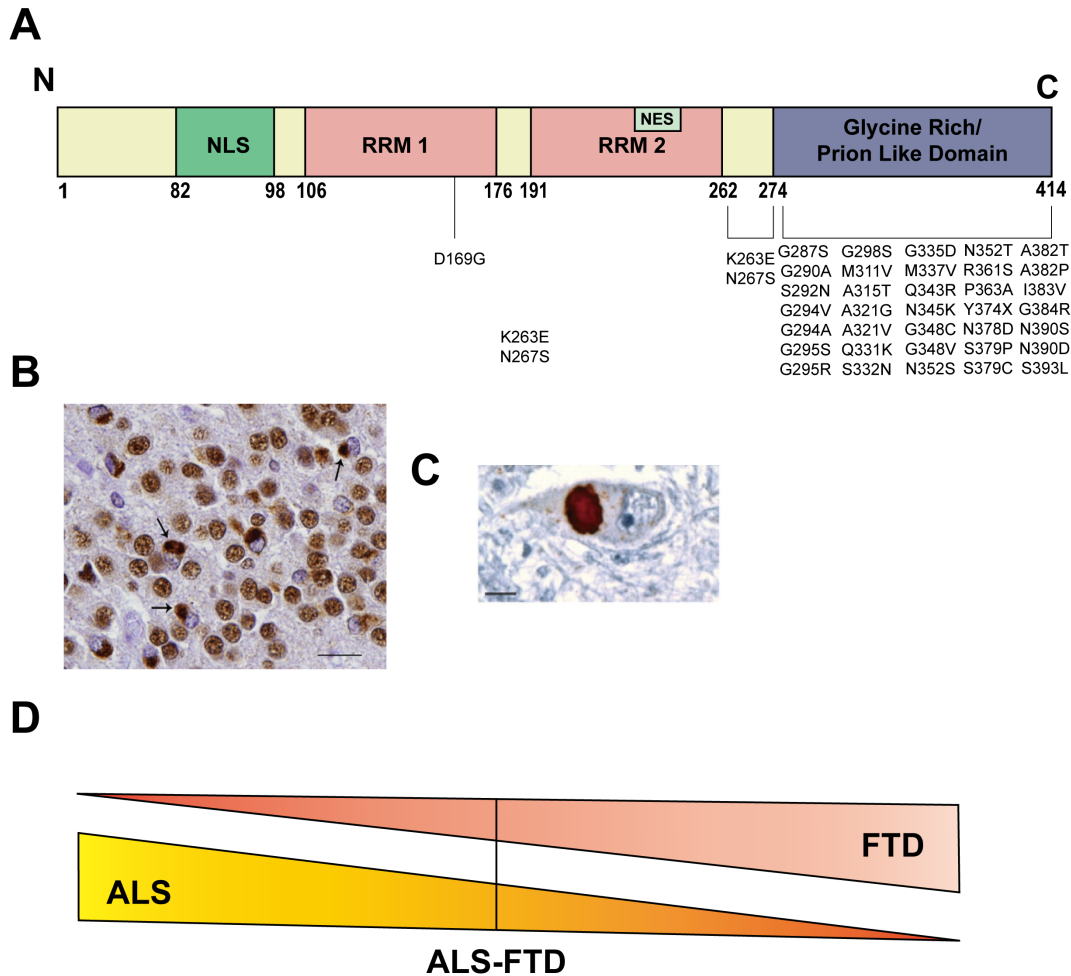
Figure 8: TDP-43 and ALS. A Schematic representation of the domain structure of TDP-43 and the TDP-43 mutations associated with ALS. **B** TDP-43 proteinopathy in neurons of brain tissue of FTLD patient (brown structures indicated by arrows) (Picture credit: Felix Geser, MD, PhD, University of Pennsylvania School of Medicine). **C** TDP-43 inclusions in motor neurons of ALS patient (Picture credit: Mackenzie et al. 2010 [68]). **D** ALS and FTD is a spectrum disorder where some patients show signs of both ALS and FTD (adapted from Swinnen and Robberecht 2014) [73].

1.6   Yeast models

Saccharomyces cerevisiae, commonly known as baker's yeast, is a eukaryotic, single-cell organism that has been frequently used as a model organism to investigate protein misfolding in a wide variety of human diseases, particularly neurodegenerative diseases ([82]). Because of the high degree of conservation of key cellular pathways and processes with mammalian cells and our vast knowledge of the yeast genome and proteome, yeast models have been widely used in scientific research and continue to pioneer studies of genetic interactions. Yeast was also the first eukaryotic organism to have its complete genome annotated and sequenced. Yeast deletion and overexpression libraries are readily available for investigating genetic interactions between certain groups of genes [13], consequently, yeast has been effectively used in high-throughput screening studies.

Studies of molecular chaperones and the heat shock response are well established in yeast models as many of the mechanisms and roles of these molecular chaperones are conserved in eukaryotes. Indeed, much of our knowledge on molecular chaperones and the heat shock response was revealed by studies using the yeast model system [12]. The molecular chaperones we investigate in this study, Hsp90 and its co-chaperones, are amongst those that have been well studied in the yeast model.

Yeast models studying many human diseases have been well-established, particularly neurodegenerative diseases and their disease proteins. This includes α-synuclein (α-syn) and parkin (PARK2) in Parkinson's Disease [83, 84], the Huntington (Htt) polyQ expansion in Huntington's Disease [85], Alzheimer's disease [86], and TDP-43 in ALS [11]. The yeast HD model is one of the most extensively characterized yeast models. It has been used to established the toxicity associated with the polyQ expansion and aggregation [85] as well as its interaction with molecular chaperones such as Hsp70 in attempts to find a therapeutic target for the disease [87].

Although yeast cells do not fully resemble neurons and thus do not display neuron-like activities, yeast cell death or growth impairment models can provide insights into neuronal cell death and studies into neurodegenerative diseases [82]. Expression of toxic proteins in yeast can result in mitochondrial damage and the production of reactive

oxygen species (ROS) that induce oxidative stress, all of which are hallmarks of many neurodegenerative disorders [88]. Another hallmark of neurodegenerative diseases, cell death from accumulation of misfolded and aggregated proteins, can also be studied in the yeast model, as misfolded proteins can induce ER stress and ROS leading to apoptotic cell death [82].

Yeast models are also widely used in ALS studies [54], including studies on SOD1, FUS, and TDP-43. In the TDP-43 yeast model, established by Johnson et al. [11, 79], TDP-43 toxicity as well as the localization and aggregation of the protein was examined, the results are summarized in Figure 9 below. The model faithfully recapitulates many central aspects of TDP-43 proteinopathy and are thus comparable to human ALS pathology, such as the cytosolic mislocalization of TDP-43 [11]. Overexpression of TDP-43 is used to model TDP-43 proteinopathy and its disease phenotypes in yeast and other animal models [1]; overexpression of the protein produces great toxicity throughout the models, supporting the role TDP-43 proteinopathy plays in gain-of-function toxicity [1]. Though there is no evidence of overexpression of TDP-43 in ALS patients, overexpression of TDP-43 in the yeast model provides a good basis to study TDP-43 proteinopathy and discover potential genetic interactions that may modify the aggregation and mislocalization of TDP-43 in cells that display TDP-43 proteinopathy.

Further investigation of TDP-43 using yeast established: 1) TDP-43 aggregation patterns in yeast cells are similar to that of ALS pathology [89], 2) TDP-43 aggregation is toxic to yeast cells, especially when expressed at high levels [89], 3) TDP-43 does not form amyloid-like aggregates [11], 4) TDP-43 aggregates differ from other protein misfolding disease proteins [11], and 5) that TDP-43 is intrinsically aggregation-prone [79].

Yeast TDP-43 Model

Aggregation

TDP-43 localizes in both the nucleus and the cytoplasm.

TDP-43 forms cytoplasmic aggregates.

TDP-43 aggregates are not amyloid-like and they are unlike other disease protein aggregates.

The C-terminal domain is required for TDP-43 aggregation, but the C-terminus alone is diffusly localized in the cytoplasm.

Toxicity

TDP-43 accumulation is toxic in yeast.

The C-terminal domain of TDP-43 is necessary for cellular toxicity, but the C-terminus alone is not sufficient for to show toxicity.

The RRM2 domain is necessary for toxicity.

Nuclear localization is not required for toxicity.

Mutants

ALS-linked TDP-43 mutations established in the yeast model:
Q331K, M337V, Q343R, N345K, R361S, and N390D

Figure 9: Characteristics of the TDP-43 yeast model summarized. The key findings and the ALS-linked TDP-43 mutants established in the TDP-43 yeast model [11, 79, 89]

1.7   Rationale, Hypothesis, Objectives, and Significance

1.7.1   Rationale

TDP-43 proteinopathy is present in the majority of ALS patients and many other neurodegenerative diseases. In TDP-43 proteinopathy, TDP-43 mislocalizes from the nucleus to the cytoplasm of neurons and forms aggregates. Protein quality control mechanisms such as molecular chaperones are utilized to combat protein misfolding, aggregation, and toxic protein species. Many studies on neurodegenerative disease have explored the interaction of disease proteins and molecular chaperones in attempt to correct the misfolding and aggregation of these proteins and find a therapeutic target for the disease. As mentioned in section 1.2.1, studies on Hsp90 as a potential target for tau aggregation in Alzheimer's disease provide a strong rationale on investigating the effects of Hsp90 and its co-chaperones on TDP-43 aggregation. We focus mostly on Sti1 in this study as previous results in the Dr. Duennwald's lab and our collaborator, Dr. Prado's lab at the University of Western Ontario, have suggested an interaction between Sti1 and TDP-43.

1.7.2   Hypothesis and Objectives

We hypothesize that Hsp90 reduces TDP-43 toxicity and aggregation through Sti1 in a dose-dependent manner. In order to test our hypothesis, we pursue three objectives:

1) To examine the effect of deletion and overexpression of Hsp90 and its co-chaperones on TDP-43 toxicity and aggregation patterns in the yeast model,

2) To establish a biochemical assay to quantify changes in aggregation patterns of TDP-43, and

3) To validate key findings our experimental results in mammalian cells.

The objectives and the methods we employ in this study are summarized in Figure 10 .
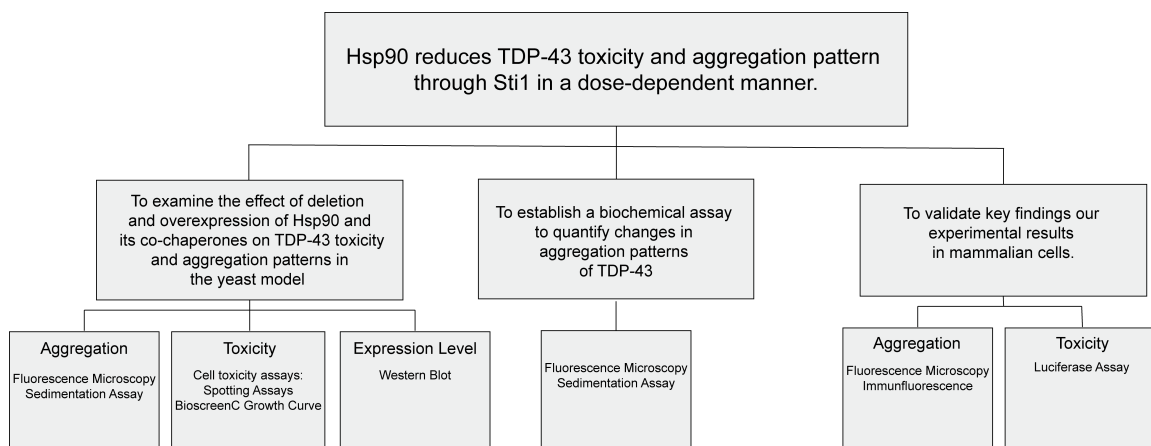
Figure 10: Graphic summary of this study.

1.7.3   Significance

In order to fully understand the pathological mechanisms underlying ALS, we must tackle the problem by focusing on fundamental mechanistic aspects, using experimentally tractable model organisms, such as yeast. These results can then be validated in neuronal systems and ALS patients. Protein aggregation generally is the hallmark of many neurodegenerative diseases, and TDP-43 proteinopathy is present in the majority of ALS and FTD cases, and a portion of patients with PD and HD. Therefore, studying TDP-43 aggregation and its interactions with molecular chaperones will provide insight in how molecular chaperones can remedy protein aggregation and eventually develop a therapeutic solution for not just ALS but possibly also other neurodegenerative diseases.

Chapter 2

2 Material and Methods

2.1 Material

2.1.1 Yeast strains and media

Yeast strain BY 4741 (MAT α *his3Δ1 leu2Δ0 lys2Δ0 ura3Δ0*) and W303 (MAT a *leu2-3,112 trp1-1 can1-100 ura3-1 ade2-1 his3-11,15*) were used in this study. Yeast deletion strains were obtained from the Saccharomyces Genome Deletion Project.

Yeast-peptone-dextrose (YPD) rich media (10 g/L yeast extract, 20 g/L peptone, and 20 g/L dextrose) and selective dextrose (SD) media (2% glucose, 1X yeast nitrogen base (YNB), 6 g/L l-isoleucine, 2 g/L L-arginine, 4g/L L-lysine HCl, 6 g/L L phenylalanine, 1 g/L L-threonine, and 1g/L L-methionine) in either liquid media or agar plates (20g/L) were used to grow yeast cells. SD media was supplemented with 4 different amino acids (4g/L L-tryptophan, 6g/L L-leucine, 2 g/L L-histidine-monohydrate) depending on the selectivity maker of the plasmid. 2% galactose or 2% galactose plus 2% raffinose was used instead of glucose as a carbon source to make selective galactose (SGal) and selective galactose raffinose (SGal Raf) media respectively, for induction of gene expression from plasmid with the GAL1 promotor.

2.1.2 E. Coli strains and media

Escherichia coli Strain DH5α Genotype F–*Φ80lacZΔM15 Δ(lacZYA-argF) 169 recA1 endA1 hsdR17 (rK–, mK+) phoA supE44 λ– thi-1 gyrA96 relA1* was used in this study. Subcloning Efficiency DH5α Competent Cells (Invitrogen, Cat. No. 18265-017) were used for the cloning work in this study.

E. Coli cultures were grown in Lysogeny Broth (LB) medium (10 g/L NaCl, 10g/L tryptone, and 5 g/L yeast extract) with antibiotic resistance (1X Ampicillin or Kanamycin depending on selectivity markers) for transformations and cloning. 2x Yeast-typtone (2xYT) media (16 g/L tryptone, 10 g/L yeast extract, and 5 g/L NaCl) was used for recovery of E. Coli cells after transformation.

2.1.3 Mammalian cell lines and media

Cervical cancer derived HeLa cells, human embryotic kidney cells (HEK), and mouse neuroblastoma cells (N2a) were used in this study. Cells were grown in Dulbecco's Modified Eagle Medium (DMEM, Corning) with 4.5 g/L and supplemented with 10% fetal bovine serum (FBS, Gibco), 1X penicillin-streptomycin solution (Corning), and 1X glutamine (Sigma Aldrich) at 37°C with ~5% CO_2. HEK wild type and HEK STI1KO cell lines were courtesy provided by the Prado Lab at Western University.

2.1.4 DNA Plasmids

pRS416Gal TDP-43 wt-YFP (low copy yeast expression plasmid) was a gift from Aaron Gitler (Addgene plasmid #27447 and 27450) [79]. The molecular chaperones for the overexpression experiments are obtained from Duennwald Lab and used to transform into pDONR201 (Invitrogen) and further into pAG423Gal-ccdB (high copy yeast expression plasmid) and pAG413Gal-ccdB (low copy yeast expression plasmid) vectors (Susan Lindquist, Addgene plasmid #14149 and 14141) through the standard Gateway Cloning protocol (Invitrogen protocol [90]), the plasmids created through Gateway cloning are summarized in the Table 2. The pEGFP wtTDP-43 plasmid was a gift from the Strong Lab at Western University and the pCMV wtSTI1 and pCFP wtSTI1 plasmids were from the Prado lab at Western University. The plasmids were transformed and purified using the Presto Midi Plasmid Kit (Geneaid). Low copy yeast expression plasmids are yeast centromere plasmids (YCp) that produce 1-2 copies of the plasmid per cell, whereas high copy yeast expression plasmids are yeast episomal plasmids (YEp) that produce about 100 copies per cell [91].

Table 2: Plasmids created using Gateway Cloning in this study

Template	Destination Vector
Sti1	pAG423Gal-ccdB
Sti1	pAG413Gal-ccdB
Cdc37	pAG423Gal-ccdB
Aha1	pAG423Gal-ccdB

2.1.5 Antibodies

The antibodies used in this study are shown in Table 3.

Table 3: Antibodies used in this study.

Antigen	Supplier	Use	Concentration
GFP	Sigma	Western Blot	1:1000
TDP-43	Sigma	Western Blot	1:1000
HA	Sigma	Immunofluorescence	1:1000
Hsp70	Thermo Fisher	Western Blot	1:2000
V5	Sigma	Immunofluorescence	1:1000
		Immunofluorescence	1:1000
Histone	Abcam	Western Blot	1:2000
PGK-1	Antibodies-online	Western Blot	1:2000
Rabbit (Alexa 680)	Life Technologies	Western Blot	1:2500
Mouse (Alexa 680)	Life Technologies	Western Blot	1:2500
Rabbit (Alexa 488)	Life Technologies	Immunofluorescence	1:1000
Mouse (Alexa 488)	Life Technologies	Immunofluorescence	1:1000
Rabbit (Texas Red)	Life Technologies	Immunofluorescence	1:1000
Mouse (Texas Red)	Life Technologies	Immunofluorescence	1:1000

2.2   Methods

2.2.1   High Efficiency Yeast Transformation

Yeast transformations were performed according to standard PEG/lithium acetate method protocol. A single colony of yeast cells are inoculated into 3 mL of YPD liquid or SD media and incubated at $30^°$C with shaking overnight. The liquid culture is then combined with 27 mL of YPD liquid to make a 30 mL liquid culture and incubated at $30^°$C shaking till the cells have reached log phase (an OD_{600} of 0.4 to 0.5). The culture is then centrifuged at 2000 xg for 5 minutes. The supernatant is aspirated off and the pellet is washed with 3 mL of sterile water. The cells are centrifuged again at the same speed and time. The pellet is resuspended in 2 mL of 100 mM Li-Acetate in TE buffer after the wash step and incubated at $30^°$C shaking for 10 minutes. The culture is centrifuged again after incubation and the pellet is resuspended in 100 μL of Li-Acetate per transformation. Each transformation is composed of 100 μL cell suspension, 250 μL transformation (1 X TE, 40% PEG, and 100mM Li-Acetate), 12μL salmon sperm DNA, 1μL (0.3~0.5 μg) plasmid DNA, and 25μl DMSO and in the order listed and vortexed thoroughly. The cells then recover at $30^°$C shaking for 30 minutes, following a 20 minute heat shock at $42^°$C shaking. After heat shock, the cells are centrifuged for 1 minute at 2000 xg, the supernatant aspirated, and the pellet resuspend in 100 μL TE buffer. The cells are then plated onto selective agar plates.

2.2.2   E. Coli Transformation

We perform E. Coli transformations to replicate and amplify plasmid DNA, resulting in abundant amounts of DNA. 100 μl aliquots of transformation competent DH5α cells are thawed on ice from storage at -80$^°$C; 1-5 μl (0.1~0.5 μg) of plasmid DNA is added to the cells and mixed thorough by gently flicking the tubes (the competent cells should not be vortexed). The cells are allowed to recover on ice for about 30 mins and heat shocked at 42$^°$C for 100 seconds. The cells rest on ice for 2 mins before 1 mL of 2xYT is added and the cells allowed to recover at 37$^°$C in a shaking incubator for at least 1 hour. Following recovery, the cells are centrifuged at 15,000 xg for one minute, the supernatant aspirated

off, and resuspend in 100 μl of 2xYT. The suspension is plated on LB agar plates with selective antibiotic depending on the antibiotic resistance of the vector.

2.2.3   Gateway Cloning

The Hsp90s and co-chaperones constructs were created through the standard procedures of Gateway cloning and consists of three steps, Polymerase Chain Reaction (PCR) amplification, BP recombination, and LR recombination following the Gateway cloning protocol developed by Invitrogen [90].

PCR was performed to obtain a template for the BP recombination reaction. We used an adapted version of the touchdown PCR program in order to avoid non-specific proliferation as a side-product of the reaction. The reaction cycle for PCR program protocol includes two cycles. The first cycle is repeated 10 times with an annealing temperature of 60° C; the second cycle is repeated 20 times with an annealing temperature of 57 $^{\circ}$C. The reaction mixture for PCR consists of 2 μl of template DNA (~200 ng), 2μl of 100 mM forward primer, 2μl of 100 mM reverse primer, 2 μl of 100 mM dNTPs, 1μl of Q5 polymerase (New England BioLabs), and 20μl of 5x Q5 buffer (New England BioLabs). The forward and reverse primers are created using the Custom Primers - OligoPerfect™ Designer (Thermo Fisher).

The BP recombination was performed by combining 2 μl of template DNA (about 100-200 ng of DNA), 1 μl of pDONR vector (150 ng/μl) , and 2 μl of 5X BP Clonase (Invitrogen). The mixture is vortexed and centrifuged twice to ensure thorough mixing and then allowed to incubate overnight at 37° C. 1 μl of Proteinase K (Invitrogen) solution is added to the reaction following incubation and left to react at 37° C for 10 minutes. 2 μl of this reaction mixture is then used to transform into Subcloning Efficiency DH5α Competent Cells (Invitrogen, Cat. No. 18265-017) following the protocol provided by the manufacturer. The cells are plated in LB Kanamycin (Kan) resistant agar plates and incubated overnight at 37° C. Colonies are picked from the plates and inoculated into LB Kan liquid overnight at 37° C. The plasmids are then extracted from the E. Coli cells by using the High-Speed Plasmid Mini Kit (Geneaid); the resulting DNA is in pDONR vector backbone.

The LR recombination reaction uses 1 µl of the product (100-300 ng) from the BP reaction in combination with 2 µl of destination vector (150 ng/µl), 13 µl of TE buffer, and 4 µl of LR Clonase (Invitrogen). The destination vectors used are listed in section 2.1.4. The mixture is vortexed and centrifuged twice and allowed to incubate overnight at 37° C. The resulting procedure is the same as described for the BP recombination reaction—Proteinase K is added to the mixture, incubated, and transformed into competent cells. The destination vectors are Ampicilin (Amp) resistant and therefore should be plated on LB Amp agar plates and then inoculated in LB Amp liquid.

All constructs are sent to the Robarts Research Institute at University of Western Ontario for DNA sequencing to verify its identity using pDONR and specifically designed sequencing primers.

2.2.4   Yeast Cell Viability Assay

Yeast cell viability is measured using two methods—spotting assays and the growth curve assay by using the BioscreenC instrument (Oy Growth Curves Ab Ltd).

2.2.4.1   Spotting Assays

Spotting assays are performed by first inoculating yeast cells in 3 mL in SD media and incubated overnight in a shaking incubator at 30° C. 100 µl of the cells are then taken in an Eppendorf tube to be diluted 1:10 in water in order to measure the OD_{600}, which indicates cell density. In a 96-well plate, we dilute our cell cultures to a cell density normalized to $OD_{600}=1$ in the first row of wells, followed by a serial dilution of 1:5 in the subsequent 5 wells. We then use a 48-prong Frogger (V&P Scientific) to spot the samples on YPD, SD, and SGal Raf plates lacking selective amino acid markers. The YPD and SD plates are used as growth and spotting controls, whereas the SGal Raf plates reflect the toxicity (e.g. of TDP-43) of the induced yeast cells. Incubation period varies with the type of plate; YPD plates are incubated 1-2 days; SD plates 2-3 days; SGal Raf plates 3-5 days. The plates are all incubated at 30° C. The plates are documented during the entire test period to monitor the growth of the yeast colonies by taking photographs using a digital camera.

Aging spotting assays were performed by inducing the yeast culture in Gal for the desired amount of days and then spotted following the procedure above.

2.2.4.2   Growth Curve Assay

The growth curve assay is performed by first inoculating yeast cells in 3 mL SD media overnight in a 30° C shaking incubator. The cells are then spun down by centrifugation and washed twice with sterile water (resuspending in water, centrifuging, and decanting the supernatant). Following the wash step, the cells are induced by resuspension in SGal media. The OD_{600} was measured by using the same procedure as described above for the spotting assays. After measuring the OD_{600}, we dilute the cells to a cell density of OD_{600}=0.2 and transfer 300 μl of the culture into corresponding wells of a honeycomb well plate. The assay runs for 3 days with 15 min read intervals. Shaking is set to turn on for 10 sec prior to the read. The incubation temperature is 30° C and the 600 nm filter is used. Prism 6 (Graph Pad) is then used to analyze the data, the replicates are averaged, and the standard deviation calculated using the available programs in Prism.

2.2.5   Fluorescent microscopy

Microscopy imaging of YFP tagged constructs was done by first inoculating yeast cells in SD media at 30° C overnight. The cells are then washed twice with sterile water, induced in SGal media, and incubated at 30° C. After inducing for 16 to 20 hours, small samples of the culture are placed on a microscope slide. The cells are imaged on Olympus BX-51 Bright Field/Fluorescence Microscope and images were captured using an equipped CCD camera (Spot Pursuit).

2.2.6   Western Blot

A 5 mL yeast culture is first inoculated in SD media overnight. The culture is then spun down at 2000 xg, washed twice, and induced in SGal media overnight. The culture is then spun down and washed once with water. The supernatant is discarded and the pellet is resuspended in 200 μl of lysis buffer (50 mM Hepes pH 7.5, 5mM EDTA, 150 mM NaCl, 1% (v/v) Triton X-100, 50 mM NEM, 2mM PMSF, and 1X Sigma protease inhibitor tablet) and transferred into an Eppendorf tube. We then add 200 μl of glass beads (ca.

500 μm in diameter) to physically disrupt the cell walls by vortexing them 6 times for 30 sec intervals and cooling on ice for 30 secs between these intervals. We then spin the culture at 5000 xg for 10 mins and collect the supernatant in a fresh Eppendorf tube.

We perform a BCA Protein Assay to determine the concentration of protein in the sample. The assay was performed according to the Thermo Scientific Pierce BCA Protein Assay Kit Instructions. After obtaining the concentration and normalizing the total protein amount in each sample per blot, we dilute the samples with 4x reducing SDS buffer (0.25M Trisma Base pH 6.8, 8.0% SDS, 40% sterile glycerol, 10% β-mercaptoethanol, 0.04% bromophenol blue).

We run SDS-PAGE with the samples on a 8-16% gradient gel (Bio-Rad Criterion TGX Stain-Free Precast Gels) and/or 12% acrylamide gels at 220 V for about 30 mins. The gel is then transferred onto a Nitrocellulose or PVDF membranes (BioRad) using the Bio-Rad Trans-Blot Turbo machine following the manufacturer's protocol. We then block the membrane using 5% skim milk powder (Carnation) in Phosphate Buffered Saline with 0.01 % (v/v) Tween (PBST) and incubating for 1 hr on a shaker. The membrane is then incubated in primary antibody overnight on shaker. Following incubation with the primary antibody, we wash the membrane with 50 ml aliquots of PBST at 10 min intervals for an hour on shaker and then incubate in the secondary antibody for 1 h on a shaker. The membrane is washed again with 50 ml aliquots of PBST in 10 min intervals on shaker for an hour. The membrane is then documented using the ChemiDoc MP System (Bio-Rad) and analyzed using Image Lab (Bio-Rad) and Prism 6 (Graph Pad).

2.2.7   Sedimentation Assay

The sedimentation assay was adapted from Theodoraki et al. (2012) and Shiber et al. (2013). A 5 mL yeast culture is first inoculated in SD media overnight. The culture is then spun down at 2000 xg, washed twice, and induced in SGal media overnight. We use $OD_{600}=1$ amount of cells from the 5 mL culture. The 1 OD_{600} culture is then further spun down and washed once with water. The supernatant is discarded and the pellet is resuspended in 200 μl of lysis (100 mM Tris, pH 7.5, 200 mM NaCl, 1 mM EDTA, 1mM DTT, 5% glycerol, 0.5% TritonX-100, 50 mM NEM, 2mM PMSF, and 1X Sigma

protease inhibitor tablet) and transferred into an Eppendorf tube. Acid-washed glass beads (425-600 μm, Sigma) are then added to physically lyse the cells by vortexing them 6 times for 30 secs intervals and cooling it on ice for 30 secs between the intervals. The tubes were pierced with a 16-gauge needle and the lysates (both pellet and supernatant) are collected in a fresh Eppendorf tube by centrifugation in pulses to separate lysates and glass beads.

The total lysates are resuspended and a BCA Protein Assay was performed to determine the concentration of total protein in the sample. The assay was performed according to the Thermo Scientific Pierce BCA Protein Assay Kit Instructions. 50 μl of the lysate was taken out and mixed with equal volume of SUMEB Buffer (8M Urea, 1% SDS, 10 mM MOPS, 10 mM EDTA, and 0.01% bromphenol blue) in a new tube, this aliquot represents total lysates. The rest of the lysate was spun down at 500 xg for 15 min at 4 °C. 100 μl of the supernatant was transferred into a new tube and mixed with 100 μl of SUMEB buffer, this represents the supernatant portion of the lysate. The remaining supernatant from the lysate was aspirated off. The pellet was resuspended with 100 μl of the lysis buffer (without protease inhibitors) and 100 μl of SUMEB buffer, this represents the pellet portion of the lysate. The samples were boiled at 80 °C for 5 min and 25 μl of the samples were loaded onto a 12% acrylamide gel. The gel is then run according to the western blot procedures described above.

2.2.8   Mammalian Cell Transfections

Mammalian cells were split into dishes or flasks with cell numbers as recommended by manufacturer and incubated for ~24 hr in DMEM. Cells were grown to approximately 90% confluency and transfected with Lipofectamine 2000 (Thermo Fisher) following the supplier recommended concentrations in Opti-MEM (Gibco) low serum media. The cells are incubated at 37 °C for 6 hr, and followed by a wash in 1X PBS and incubated in DMEM for ~20 hr at 37 °C. Cells are then split into different dishes or plates for different experimental setups. Plates destined to contain HEK cells were treated with Attachment Factor (Gibco) to prevent detaching of cells. HEK and N2a cells were transfected with Lipofectamine LTX with Plus Reagent (Thermo Fisher) following the supplier

recommended concentrations. HEK cells were transfected directly into 96 well plates for the viability assay and chamber slides for immunofluorescence microscopy.

2.2.9   Mammalian Cell Viability Assay

The CellTiter-Glo Luminescent Cell Viability Assay (Promega) was used in this study. This assay delivers a highly sensitive read out of cellular fitness and is particularly useful for studies on the toxicity associated with misfolded proteins. Transfected cells are split into 96 well plates and grown in DMEM (Corning) for HeLa cells or mimimum DMEM with 1% fetal bovine serum (FBS, Gibco) and 1 g/L glucose for HEK and N2a cells. This minimal medium increases sensitivity to the toxic effects of protein misfolding in many other systems [92], as well as differentiating N2a cells [93]. The cells are incubated at 37 °C for 20~24 hr. The cell viability assay is then performed according to the supplier's instructions. Plates were then measured using the Victor3V Plate Reader (Perkin Elmer) using the Perkin Elmer 2030 Manager Software. Viability assays on N2a cells were measured using the Cytation 5 Cell Imaging Multi-Mode Reader (Biotek).

2.2.10   Immunofluorescence Microscopy

Following transfection, the cells are split into 8 well chambers (Labtek) and grown in DMEM at 37 °C for 20~24 hr. Each well is seeded with ca. 30,000 cells. The media is then aspirated off and the cells washed 2 times with PBS. 4% paraformaldehyde is then added to the wells to fix the cells for 15 min. This is followed by 3 washes in PBS. The cells are permeablized with 0.5% TritonX-100 in PBS for 15 mins and washed with PBS 3 times, followed by 5 washes in 0.5% BSA (Sigma) in PBS (PBB). We block non-specific binding sites with 20% normal goat serum (Gibco) in PBB for 45 min. The cells are then washed with PBB 5 times and incubated for an hour in mouse α-GFP (Sigma) as well as rabbit α-Hsp90 (Proteintech) primary antibody for Hsp90 co-localization studies. We wash the cells with PBB 5 times and incubate for an hour in goat α-mouse alexa-488 and/or α-rabbit texas red secondary antibody (Thermo Fisher). Following the secondary antibody incubation, we wash in PBB 5 times. All the liquid is then aspirated off and mounted with ProLong® Gold Antifade Mountant with DAPI. The cells are imaged on a Zeiss Axiovert A1 wide-field fluorescent micrope with a AxioCam ICm 1 R1 CCD

camera (Carl Zeiss). N2a cells were imaged with the Cytation 5 Cell Imaging Multi-Mode Reader (Biotek).

2.2.11   Statistical Analysis

Statistical analysis of the growth curve assays, viability assays, and the western blots were done using the GraphPad Prism 6 software. Statistical significance was obtained by performing unpaired t-tests to compare the means and standard deviations between the control data set and the experiment data set (each at a minimum of three biological replicas). Significance levels are indicated using asterisks, where **** is $p<0.0001$, *** is $p<0.001$, ** is $p<0.01$, * is $p<0.05$.

Chapter 3

3   Results

3.1   The TDP-43 yeast model

We use spotting assays and growth curve assays to determine cellular toxicity in yeast cells. Reduction of growth rates is a well-established read out for the toxicity associated with protein misfolding in yeast models [11, 85, 94]. Spotting assays allow us to visualize cellular toxicity by juxtaposing different constructs diluted 1:5 side by side and assess the difference in growth, while growth curve assays provide quantitative results for cellular toxicity by comparing the growth curves of different constructs at different growth stages (lag, mid-logarithmic, and stationary phase). The combination of spotting assay and growth curve assay offers a more comprehensive understanding of the growth of different constructs, allowing us to infer cellular toxicity. All experiments in this study were performed with a minimum of at least three biologically distinct constructs unless otherwise specified (i.e. minimum of three biological replicates).

The TDP-43 construct used in this study contains human wild type TDP-43 fused to yellow fluorescent protein (YFP, schematic is shown in Figure 11A). We refer to TDP-43^{WT}-YFP as TDP-43 in the rest of this thesis. Spotting assays were performed with yeast cells expressing TDP-43 show diminished growth, suggesting toxicity of TDP-43 in yeast (Figure 11B). The same toxicity is replicated in the growth curve assay (Figure 11C). When the TDP-43 expressing yeast cells are viewed under fluorescent microscopy, we observe TDP-43 expression in both the nucleus and the cytoplasm. Cytoplasmic aggregates are also present in cells, recapitulating TDP-43 proteinopathy as observed in motor neurons of ALS patients and many model organisms. Our results thus reproduce the previously published results introducing the TDP-43 yeast model using our own expression vectors [11].

The results shown in this study are obtained by using the BY 4741 (MAT α) yeast strain, which is commonly used in protein misfolding studies [54] unless otherwise stated. Molecular chaperone overexpression experiments have additionally been performed in the yeast W303 (MAT a) strain (another yeast strain commonly used for protein misdfolding studies), the results of which are shown in the supplement section of this study.

A

B

C

D
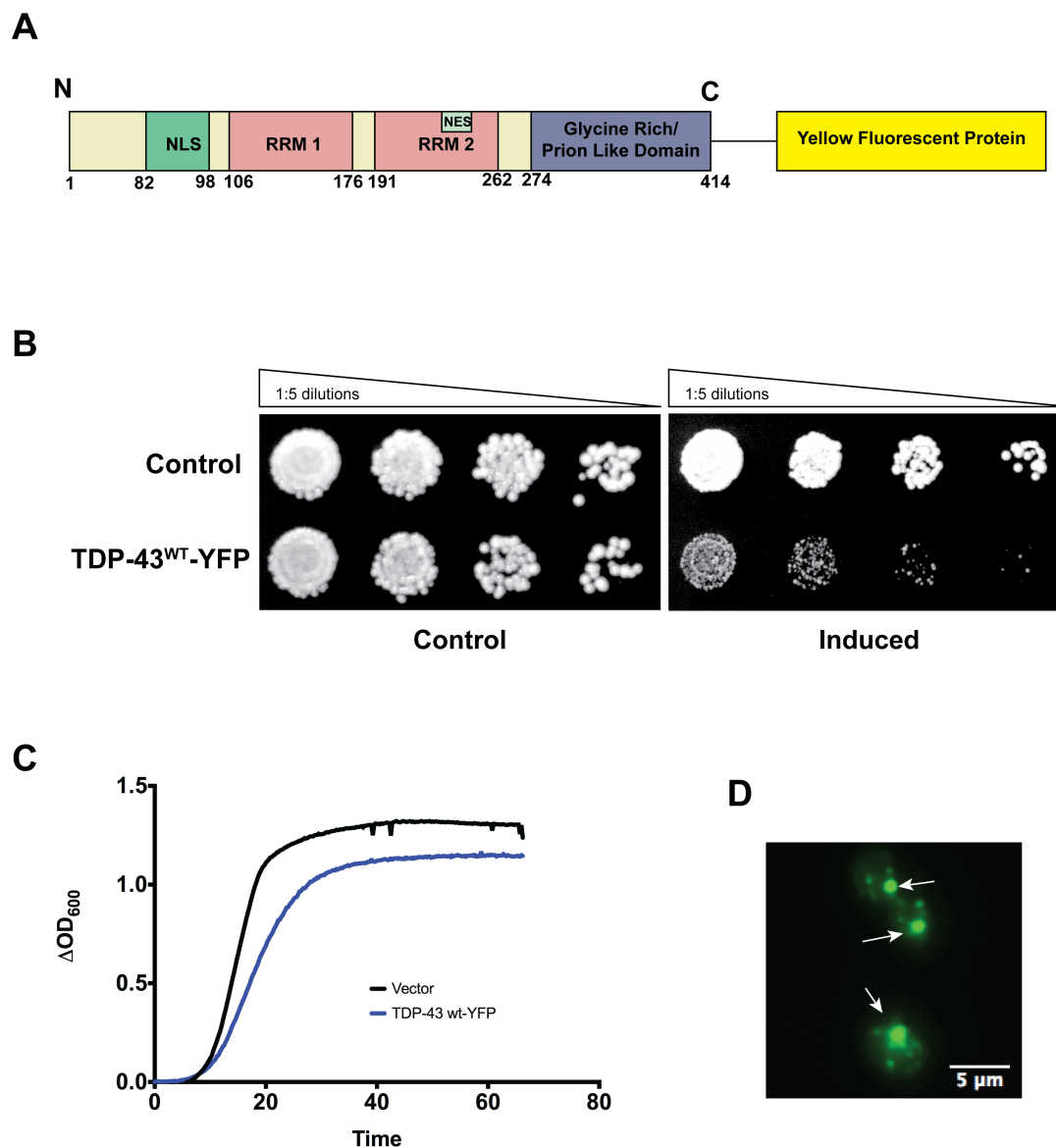
Figure 11: TDP-43 yeast model. A Schematic representation of the TDP-43 wild type construct fused with the yellow fluorescent protein (YFP). **B** Spotting assay showing TDP-43 toxicity when induced. **C** Growth curve assay showing TDP-43 toxicity of significance level p<0.0001. **D** Fluorescence microscopy image of TDP-43^{WT}-YFP in BY (MAT α) showing TDP-43 expression in both the nucleus (white arrowheads) and the cytoplasm with cytoplasmic inclusions.

3.2   Sedimentation Assay

Although the localization and aggregation patterns of TDP-43 can be visualized using fluorescence microscopy, the changes in these patterns could not be fully characterized and quantified by using microscopic methods alone. TDP-43 aggregates have been especially difficult to characterize biochemically since TDP-43 has been described as "sticky" yet rather soluble [79], making it a challenge to quantify or characterize the changes in aggregation using conventional methods, such as filter retardation assays or semi-denaturing detergent agarose gel electrophoresis (SDD-AGE). To devise a reproducible and quantitative biochemical assay to determine TDP-43 aggregation, we have established here a novel sedimentation assay based on the solubility analysis assays of Theodoraki et al. (2012) [95] and Shiber et al. (2013)[96].

The sedimentation assay divides cellular protein lysates into two fractions, the pellet, which represents the insoluble portion of the lysate, and the supernatant, which represents the soluble portion of the lysate. The two fractions of the lysate were loaded onto a polyacrylamide (SDS-PAGE) gel along with a sample of the total lysate to ensure equal expression level. A detailed protocol of this assay is provided under Material and Methods in this thesis.

We first performed the sedimentation assay on various TDP-43 constructs and compared them with fluorescence microscopy images. We observe that our TDP-43 construct expresses mostly insoluble TDP-43 aggregates (Figure 12A). Using yeast strain W303 with various integrated TDP-43 expression levels (1X, 2X, 3X) fused with a green fluorescence protein (GFP) [11], we observe that 1X TDP-43 is expressed at such low levels that is difficult to detect by immunoblotting (Figure 12B) and the low protein levels shown by the sedimentation assay blots correspond to the low intensity of the fluorescence microscopy of the construct. The 2X and 3X TDP-43 constructs (Figure 12 C and D) show, as expected, higher-level expression levels compared to the 1X TDP-43. We quantify the sedimentation assay blots of 2X and 3X TDP-43 and compare the difference in pellet-to-supernatant ratio (Figure 12H). 3X TDP-43 is shown to have a smaller pellet-to-supernatant ratio, indicating more soluble TDP-43 in the lysate.

These results of the sedimentation assay correspond to the fluorescent microscopy images: 3X TDP-43 produces more diffuse signal throughout the cell (cytosol and nucleus) as shown in Figure 12D. The sedimentation assay was also performed on yeast cells expressing TDP-43 and empty vector (Figure 12G) and the blots probed with α- and α-histone antibody as loading controls. The results show that the distribution of PGK-1 and histone does not change whether TDP-43 is expressed or not and therefore PGK-1 and histones can serve as proper loading controls for this assay.

We next tested whether the same protocol can also serve to monitor TDP-43 aggregation in cultured mammalian cells. To this end, HeLa cells expressing GFP alone and eGFP-TDP-43 were lysed following the sedimentation assay protocol outlined above with minimal adjustments for mammalian cell lysis (see Materials and Methods). As expected, in GFP-expressing HeLa cells (Figure 12E), GFP appears dispersed throughout the cell and forms no aggregates, which corresponds to the sedimentation assay results where GFP protein is mostly soluble (Figure 12E and I). In contrast, TDP-43 was localized predominately in the nucleus of HeLa cells and formed nuclear aggregates (Figure 12F and I). The results show TDP-43 to be completely insoluble in HeLa cell lysates. Thus, HeLa cell sedimentation assay results correspond well to the microscopy results performed on the same cell and constructs.

A

TDP-43

Total   Pellet   Supernatant

5 µm   5 µm

B

Total   Pellet   Supernatant

1X TDP-43-GFP

5 µm

C

Total   Pellet   Supernatant

2X TDP-43-GFP

5 µm

D

Total   Pellet   Supernatant

3X TDP-43-GFP

5 µm

E

Total   Pellet   Supernatant

20 µm

F

Total   Pellet   Supernatant

20 µm

G

		Total	Pellet	Supernatant
PGK-1	Control			
	TDP-43			
Histone	Control			
	TDP-43			

H

Pellet:Supernatant

2X TDP-43   3X TDP-43

I

Pellet:Supernatant

PEGFP   PEGFP TDP-43
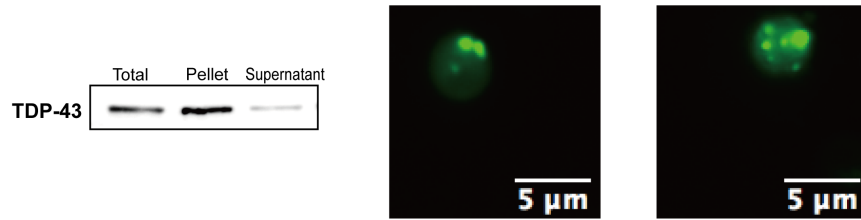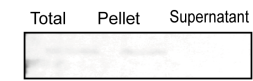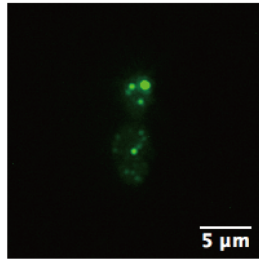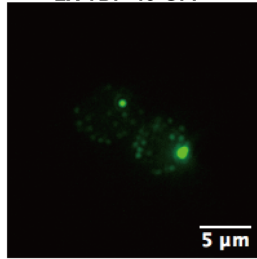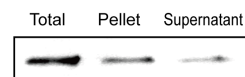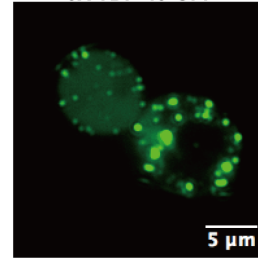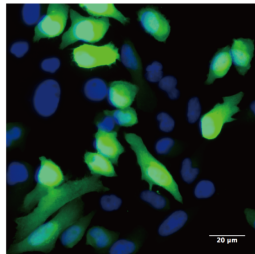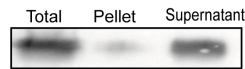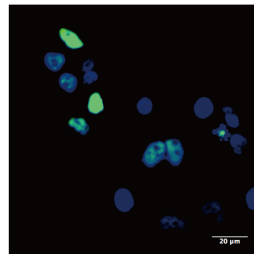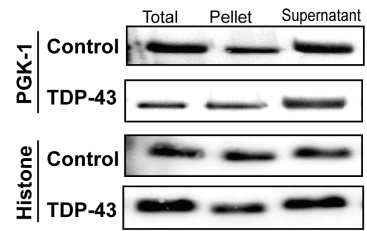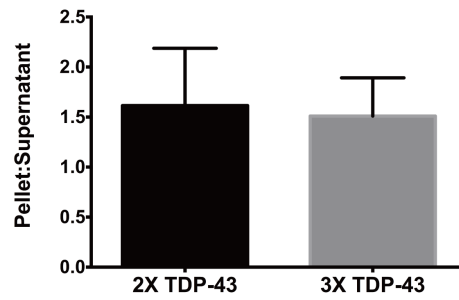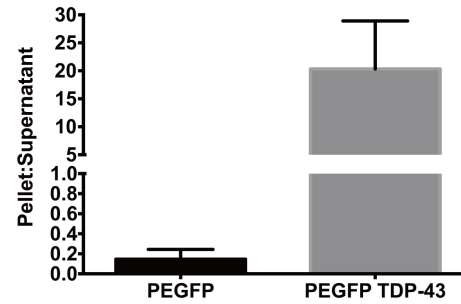
Figure 12: Sedimentation assay and fluorescence microscopy of yeast cells expressing various TDP-43 constructs at different levels. Sedimentation assay and fluorescence microscopy images of **A** TDP-43^{WT}-YFP in BY (MAT α) yeast cells, **B** integrated 1X TDP-43^{WT}-GFP in W303 (MAT a) yeast cells, **C** integrated 2X TDP-43^{WT}-GFP in W303 (MAT a) yeast cells, **D** integrated 3X TDP-43^{WT}-GFP in W303 (MAT a) yeast cells, **E** eGFP in HeLa cells, and **F** eGFP-TDP-43 in HeLa cells. **G** Sedimentation assay of vector control and TDP-43^{WT}-YFP in BY (MAT α) yeast cells probed with α-PGK-1 and α-histone antibody. Statistical analysis of the pellet-to-supernatant ratio of the sedimentation results of **H** 2X TDP-43^{WT}-GFP and 3X TDP-43^{WT}-GFP in W303 (MAT a) yeast cells and **I** eGFP and eGFP-TDP-43 in HeLa cells.

Next, we sought to assess whether the sedimentation assay can also serve to follow the shift of molecular chaperones to a more insoluble subcellular fraction under stress conditions that elicit protein misfolding and aggregation. Previous microscopic studies have shown that molecular chaperones can associate closely with such misfolded and aggregated proteins [19]. We performed the sedimentation assay on wild type yeast cells and applied protein folding stress chemically with azetidine-2-carboxylic acid (AZC) and by heat shock. AZC is an analog of proline and is able to reduce the thermal stability or lead to misfolding when competitively incorporated into proteins in place of proline [97]. The misfolding of these proteins induces protein-folding stress and activates the heat shock response in the cell. Proteins that have AZC incorporated have also been reported to misfold and aggregate and show increased binding affinity to Hsp70 [97]. We treat wild type cells with 2mM AZC for four hours or heat shock at 42 °C for one hour in order to observe a potential shift from a soluble to a more insoluble fraction of different molecular chaperones due to association of the chaperones with misfolded and aggregated proteins using the sedimentation assay.

First, we cultured wild type cells in YPD overnight and treated with AZC or heat shock and probed the sedimentation analysis blots with an anti-Hsp70 antibody. The Hsp70 family of cytosolic molecular chaperones is responsible for protein folding, the assembly of newly synthesized protein, and solubilizing protein aggregate and can be up-regulated under stress conditions to combat protein misfolding and aggregation [98]. The results are shown in Figure 13A. However, the statistical analysis of these results (Figure 13B) did not show significance. This may be due to the very high abundance of Hsp70 in the cell under normal and stress conditions. Therefore the effect of a shift to a more insoluble subcellular fraction of Hsp70s cannot be clearly observed in the sedimentation assay.

Next, we probed cells with α-Hsp104 antibody instead as it is less abundant than Hsp70s. Hsp104 is a protein remodeling factor that cooperates with Hsp70s and Hsp40s to promote the refolding of denatured proteins and acts as a disaggregase to pull apart protein aggregates [99]. Thus, as demonstrated by microscopic studies, Hsp104, is closely associated with misfolded and aggregated proteins to mitigate the toxic effects of protein aggregation and misfolding [100]. The results in Figure 13C show that the

distribution of pellet-to-supernatant did not show significant change between the stressed and unstressed samples (Figure 13D). We speculated that stress treatment of cells in the extremely rich medium YPD did not elicit severe cellular stress due to high cell division rates. We therefore cultured wild type cells in SD media (a medium with less nutrients than YPD) overnight instead and stressed them under the same stress conditions. The results in Figure 13E show that the distribution of pellet-to-supernatant also did not show a significant change between the stressed and no stress samples (Figure 13F).

We also explored whether the sedimentation assay can detect localization changes in of molecular chaperones in cultured mammalian cells. To this end, HeLa cells were treated with 10 mM AZC and 20 μM carbobenzoxy-L-leucyl-L-leucyl-L-leucinal (MG132) for one hour and the sedimentation assay blots were probed with an anti-Hsp70 antibody. MG132 is a protease inhibitor that inhibits the 26S proteasome complex in cells, resulting in protein misfolding and aggregation [101]. The results of AZC and MG132 treatment of HeLa cells are shown in Figure 13G. We observe no statistically significant change in Hsp70 solubility (Figure 13F).
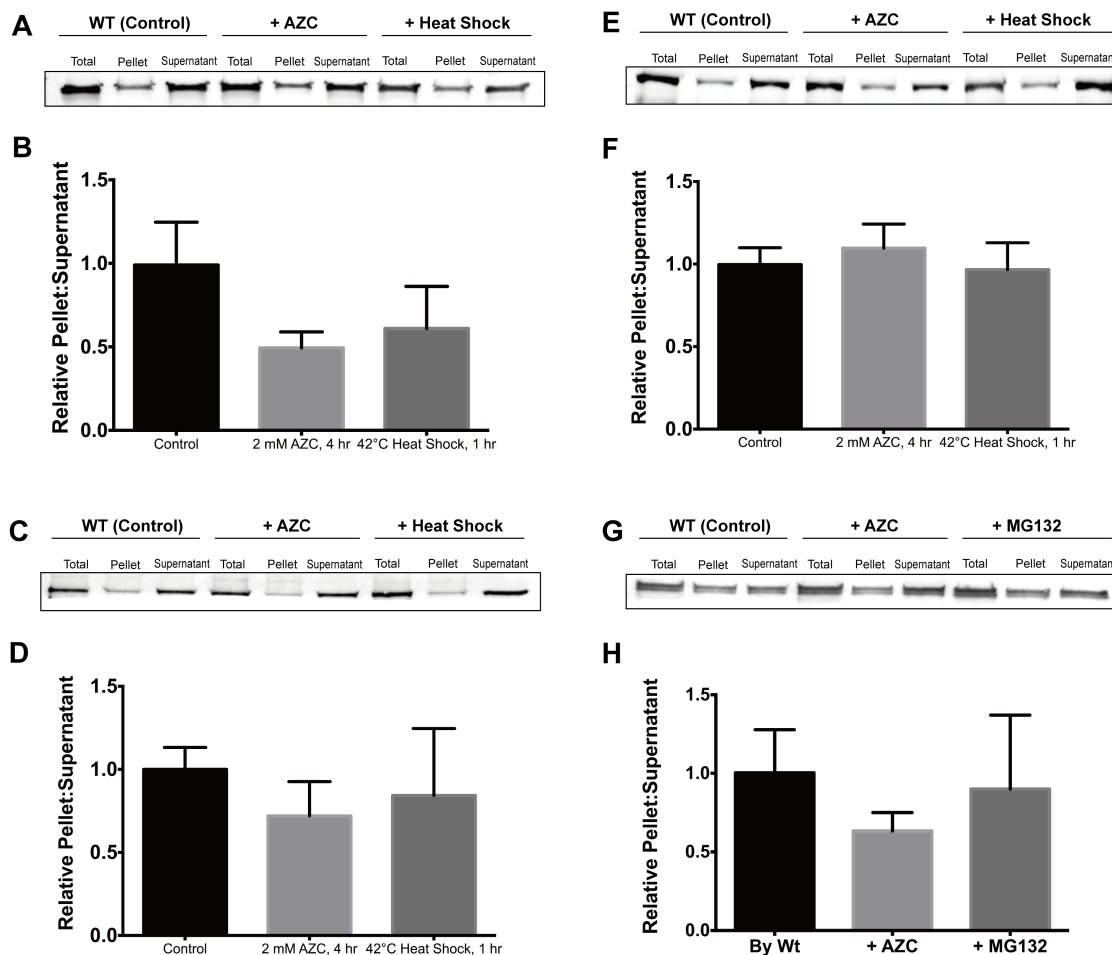
Figure 13: **Sedimentation assays of stress treated wild type yeast and HeLa cells.** Sedimentation assay blots and statistical analyses of wild type yeast cells grown in YPD and probed with α-Hsp70 antibody (**A** and **B**) and α-Hsp104 antibody (**C** and **D**). The sedimentation assay blots and statistical analysis of wild type yeast cells grown in SD and probed with α-Hsp104 antibody (**E** and **F**). The sedimentation assay blots and statistical analysis of wild type HeLa cells probed with α-Hsp70 antibody (**G** and **H**).

3.3 Hsp90 modulates TDP-43 stability, aggregation, and toxicity in yeast

3.3.1   Hsc82 and TDP-43

We expressed TDP-43 and an empty vector as control in yeast cells that lacked the Hsc82 encoding gene (*hsc82Δ*), which is the constitutively expressed allele of Hsp90 in yeast. Growth assays and fluorescence microscopy were performed on *hsc82Δ* cells to observe TDP-43 toxicity and aggregation. Spotting assays show a slight increase in toxicity when compared to wild type yeast cells expressing TDP-43 (Figure 14A). However, this slight increase in toxicity is not reproduced in the growth curve assay (Figure 14B) as these results are not statistically significant. Fluorescence microscopy results show no significant difference in aggregation pattern of TDP-43 in *hsc82Δ* cells when compared to wild type cells (Figure 14C). Western blots of the two TDP-43 expressing constructs show no difference in TDP-43 expression level (Figure 14G).

Overexpression of Hsc82 using a high copy plasmid in TDP-43 expressing wild type yeast cells show significant increase in toxicity in both the spotting assay (Figure 14D) and the growth curve assay (Figure 14E). Fluorescence microscopy results show no change in aggregation patterns (Figure 14F), which is corroborated by sedimentation assays (Figure 14H). Notably, western blots show a significant increase in TDP-43 expression level upon Hsc82 overexpression (Figure 14G and I).

A

1:5 dilutions

1:5 dilutions

Wild Type — Control / TDP-43

hsc82Δ — Control / TDP-43

Control   Induced

B

ΔOD$_{600}$ vs Time

- Vector (Control)
- hsc82Δ Vector
- TDP-43
- hsc82Δ TDP-43

C

5 μm

D

1:5 dilutions

1:5 dilutions

Wild Type — Control / TDP-43

+Hsc82 — Control / TDP-43

Control   Induced

E

ΔOD$_{600}$ vs Time

- Vector (Control)
- TDP-43
- Vector + Hsc82
- TDP-43 + Hsc82

****

F

5 μm

G

TDP-43

	WT	hsc82Δ
TDP-43		
PGK1		

TDP-43

	+ Vector	+Hsc82
TDP-43		
PGK1		

H

TDP-43

	Total	Pellet	Supernatant
+ Vector			
+ Hsc82			

I

TDP-43:PGK-1(%)

****

+Vector   +Hsc82

Figure 14: Hsc82 and TDP-43 interaction in yeast. **A** Spotting assays of wild type and *hsc82Δ* cells expressing TDP-43. **B** Growth curve assays of wild type and *hsc82Δ* cells expressing TDP-43. **C** Fluorescence microscopy of TDP-43 expressing *hsc82Δ* cells. **D** Spotting assays of TDP-43-expressing wild type cells overexpressing Hsc82. **E** Growth curve assays of TDP-43-expressing wild type cells overexpressing Hsc82. The significance level is $p < 0.0001$. **F** Fluorescence microscopy of TDP-43-expressing wild type cells overexpressing Hsc82. **G** Western blots showing TDP-43 expression level of wild type and *hsc82Δ* cells and wild type cells overexpressing Hsc82. **H** Sedimentation assay of TDP-43-expressing wild type cells overexpressing Hsc82. **I** Statistical analysis of the western blots showing TDP-43 expression level of cells overexpressing Hsc82 with a significance level of $p < 0.0001$.

3.3.2   Hsp82 and TDP-43

In yeast cells that lacked the Hsp82 encoding gene (*hsp82Δ*), spotting assay results show a slight rescue in TDP-43 toxicity (Figure 15A). This rescue increase in toxicity is not observed in the growth curve assay as *hsp82Δ* cells expressing TDP-43 grow similarly to wild type cells (Figure 15B). Fluorescence microscopy results show no significant difference in aggregation pattern of TDP-43 in *hsp82Δ* cells when compared to wild type cells (Figure 15C). Western blots of the two TDP-43 expressing constructs show no difference in TDP-43 expression level (Figure 15G).

Overexpression of Hsp82 using a high copy plasmid in TDP-43 expressing wild type yeast cells show significant increase in toxicity in both the spotting assay (Figure 15D) and the growth curve assay (Figure 15E). Fluorescence microscopy results show no change in aggregation pattern (Figure 15F), which is corroborated by the sedimentation assay (Figure 15H). Notably, western blot results also show a significant increase in TDP-43 expression level when Hsp82 is overexpressed, similar to the increased TDP-43 levels in Hsc82 overexpressing cells (Figure 15G and I).

A

B

C

D

E
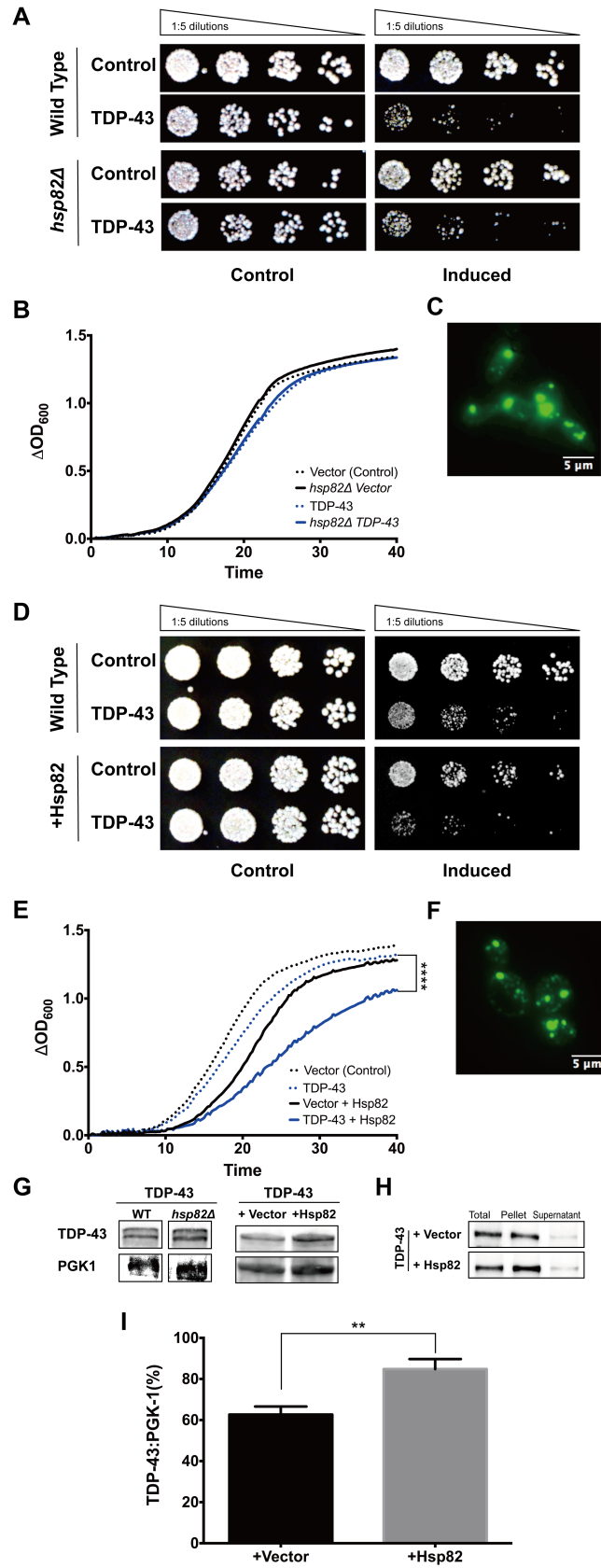

F

G

H

I

Figure 15: Hsp82 and TDP-43 interaction in yeast. **A** Spotting assays of wild type and *hsp82Δ* cells expressing TDP-43. **B** Growth curve assays of wild type and *hsp82Δ* cells expressing TDP-43. **C** Fluorescence microscopy of TDP-43 expressing *hsp82Δ* cells. **D** Spotting assays of TDP-43-expressing wild type cells overexpressing Hsp82. **E** Growth curve assays of TDP-43-expressing wild type cells overexpressing Hsc82. The significance level is p<0.0001. **F** Fluorescence microscopy of TDP-43-expressing wild type cells overexpressing Hsp82. **G** Western blots showing TDP-43 expression level of wild type and *hsp82Δ* cells and wild type cells overexpressing Hsp82. **H** Sedimentation assay of TDP-43-expressing wild type cells overexpressing Hsp82. **I** Statistical analysis of the western blots showing TDP-43 expression level of cells overexpressing Hsc82 with a significance level of p=0.0036.

3.4 Hsp90 co-chaperones and TDP-43

We next tested the effect of the Hsp90 co-chaperones Aha1, Cdc37 and Sti1 on TDP-43 toxicity, localization, aggregation, and protein levels in yeast.

3.4.1   Aha1

In *aha1Δ* cells, both spotting assay and growth curve results show no change in TDP-43 toxicity, as wild type and *aha1Δ* cells grow at highly similar rates (Figure 16A and B). Fluorescence microscopy results show no significant difference in aggregation pattern of TDP-43 in *aha1Δ* cells when compared to wild type cells (Figure 16F). Western blots of the two TDP-43 expressing constructs show no difference in TDP-43 expression level (Figure 16G).

Overexpression of Aha1 using a high copy plasmid in TDP-43 expressing wild type yeast cells show significant increase in TDP-43 toxicity in both the spotting assay (Figure 16D) and the growth curve assay (Figure 16E). Fluorescence microscopy and sedimentation assay results show no change in aggregation pattern (Figure 16F and H). Western blot results show no significant change in expression level of TDP-43 due to Aha1 overexpression (Figure 16G).

A

Wild Type — Control, TDP-43
aha1Δ — Control, TDP-43

Control | Induced

B

ΔOD_{600} vs Time

- Vector (Control)
- *aha1Δ Vector*
- TDP-43
- *aha1Δ TDP-43*

C

5 µm

D

Wild Type — Control, TDP-43
+Aha1 — Control, TDP-43

Control | Induced

E

ΔOD_{600} vs Time

- Vector (Control)
- TDP-43
- Vector + Aha1
- TDP-43 + Aha1

****

F

5 µm

G

TDP-43

| | WT | *aha1Δ* | + Vector | +Aha1 |
TDP-43
PGK1

H

TDP-43 + Vector / + Aha1

Total | Pellet | Supernatant
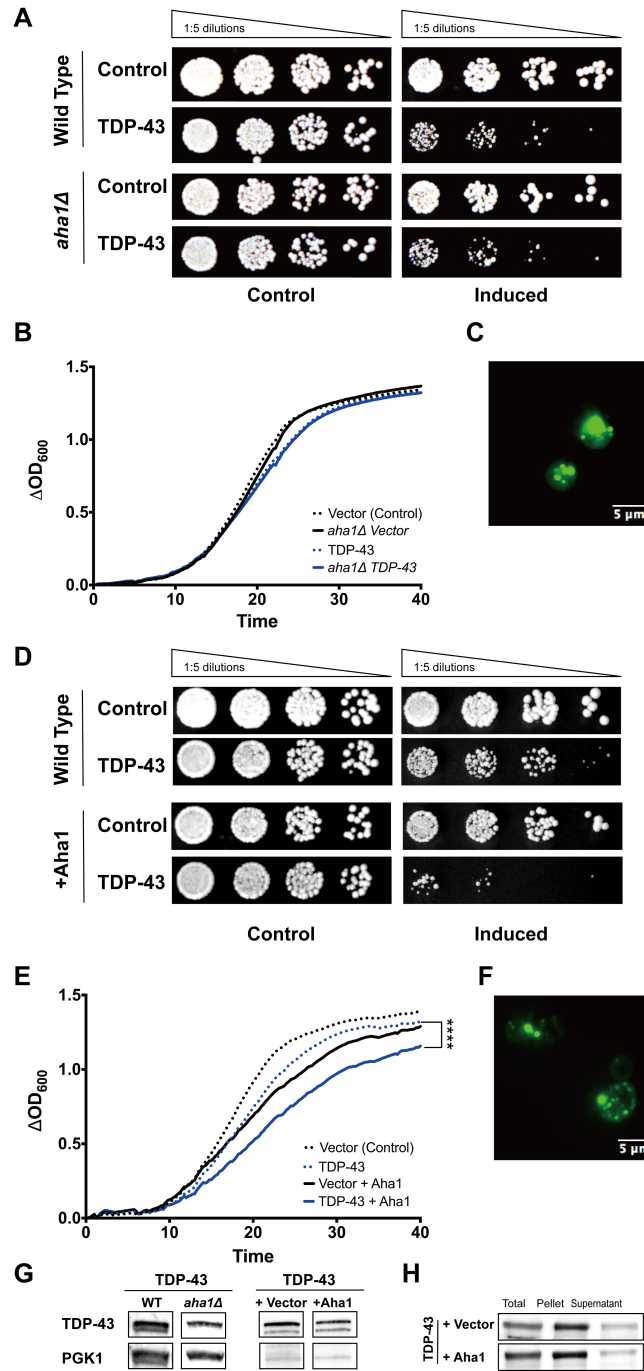
Figure 16: Aha1 and TDP-43 interaction in yeast. **A** Spotting assays of wild type and *aha1Δ* cells expressing TDP-43. **B** Growth curve assays of wild type and *aha1Δ* cells expressing TDP-43. **C** Fluorescence microscopy of TDP-43 expressing *aha1Δ* cells. **D** Spotting assays of TDP-43-expressing wild type cells overexpressing Aha1. **E** Growth curve assays of TDP-43-expressing wild type cells overexpressing Aha1. The significance level is p<0.0001. **F** Fluorescence microscopy of TDP-43-expressing wild type cells overexpressing Aha1. **G** Western blots showing TDP-43 expression level of wild type and *aha1Δ* cells and wild type cells overexpressing Aha1. **H** Sedimentation assay of TDP-43-expressing wild type cells overexpressing Aha1.

3.4.2   Cdc37 and TDP-43

Cdc37 is essential for the survival of yeast and cannot be deleted from its genome, therefore yeast cells lacking Cdc37 expressing TDP-43 could not be obtained. Overexpression of Cdc37 using a high copy plasmid in TDP-43 expressing wild type yeast cells show significant increase in toxicity in both spotting assays (Figure 17A) and growth curve assays (Figure 17B). Fluorescence microscopy and sedimentation assay results show no change in aggregation pattern (Figure 17C and E). Western blot results show a decrease in expression level of TDP-43 in some biological replicates (Figure 17D), while others showed no change in TDP-43 expression level (data not shown).
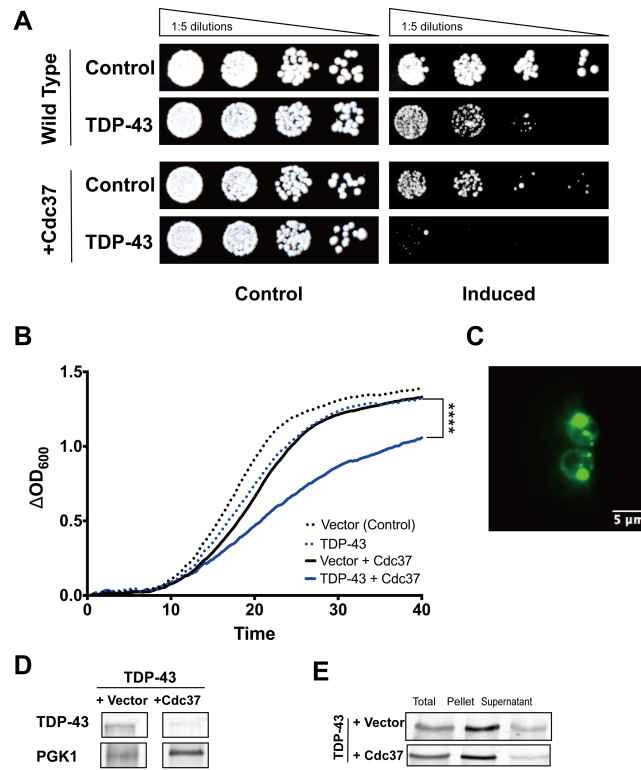
Figure 17: Cdc37 and TDP-43 interaction in yeast. A Spotting assay of TDP-43-expressing wild type cells overexpressing Cdc37. **B** Growth curve assay of TDP-43-expressing wild type cells overexpressing high copy Cdc37 with significance level $p<0.0001$. **C** Fluorescence microscopy TDP-43-expressing wild type cells overexpressing Cdc37. **D** Western blots showing TDP-43 expression level of wild type cells overexpressing high copy Cdc37. **E** Sedimentation assay of TDP-43-expressing wild type cells overexpressing high copy Cdc37.

3.4.3   Sti1 and TDP-43

In *sti1Δ* cells, spotting assay show no change in toxicity compared to the wild type cells (Figure 18A), however, growth curve results show a prolonged lag phase of *sti1Δ cells* expressing TDP-43 (Figure 18B). The growth of *sti1Δ* constructs were tested at 37 °C and showed a growth phenotype consistent with previously published results [42](Figure 18D), thus providing evidence that our *sti1Δ* show a proper characteristic phenotype. The effect of chronological aging on TDP-43 expressing *sti1Δ* was also tested. Here, chronological aging serves a physiologically relevant stress condition that can sensitize yeast cells to the toxicity associated with protein misfolding. Our results show that when TDP-43 expression has been induced for four days, the viability of cells expressing TDP-43 was decreased since a reduced number of cells grow back into colonies on control plates (Figure 18F). Interestingly, *sti1Δ* cells harboring the empty vector control seem to be growing better than the wild type cells, indicating that the cells have up-regulated other cellular mechanisms to combat the lack of Sti1 in aging. On day six of the aging assay (Figure 18G) we observe that TDP-43 constructs lose its toxicity, indicating that the yeast cells have stopped expressing TDP-43. However TDP-43 expressing *sti1Δ* cells continue to show great toxicity. Fluorescence microscopy results of the *sti1Δ* construct show less cytoplasmic TDP-43 aggregates compared to wild type cells (Figure 18C). Western blots of the two TDP-43 expressing constructs show no difference in TDP-43 expression level (Figure 18E).

A

B

C

D

E

F

G

H
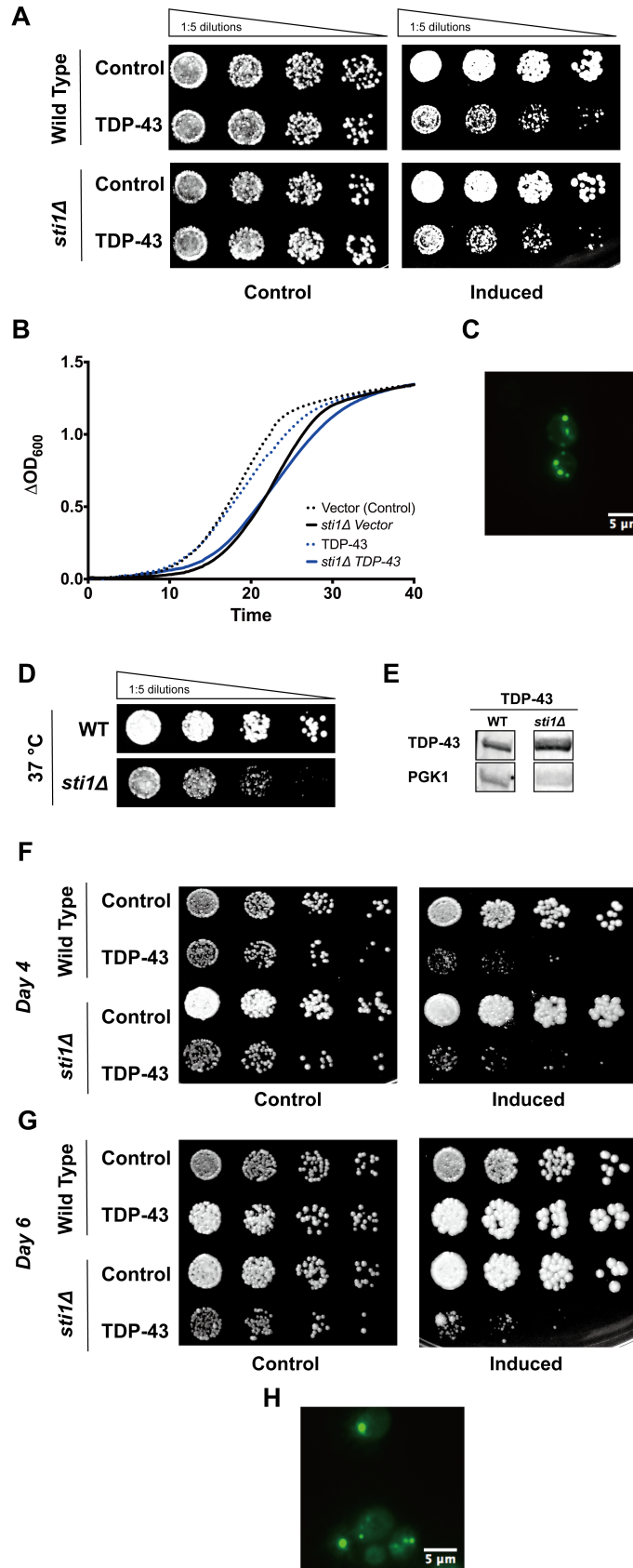
Figure 18: Sti1 and TDP-43 interaction in yeast – *sti1Δ*. **A** Spotting assay of wild type and *sti1Δ* cells expressing TDP-43. **B** Growth curve assay of wild type and *sti1Δ* cells expressing TDP-43. **C** Fluorescence microscopy of TDP-43 expressing *sti1Δ* cells. **D** Spotting assay of wild type and *sti1Δ* cells expressing an empty vector at 37 °C. **E** Western blots showing TDP-43 expression level of wild type and *sti1Δ* cells. **F** Day 4 of aging spotting assay of wild type and *sti1Δ* cells expressing TDP-43. **G** Day 6 of aging spotting assay of wild type and *sti1Δ* cells expressing TDP-43. **H** Fluorescence microscopy of *sti1Δ* cells expressing TDP-43 after 4 days of induction.

Overexpression of Sti1 using a high copy plasmid in TDP-43 expressing wild type yeast cells show only a slight increase in toxicity in spotting assays compared to the other molecular chaperones (Figure 19A). On the other hand, a significant increase in toxicity is shown in growth curve assays (Figure 19B). Fluorescence microscopy results show less TDP-43 aggregates in the cytoplasm when Sti1 is expressed (Figure 19C).

We conduct the same experiments by using the low copy Sti1 plasmid instead to further discern the changes in TDP-43 toxicity and aggregation and its interaction with Sti1. Spotting assay results with the low copy overexpression of Sti1 show no change in toxicity (Figure 19D), but the growth curve results show a significant rescue in toxicity (Figure 19E). The fluorescence microscopy results show more soluble TDP-43 in the cytoplasm (Figure 19F), which is corroborated by sedimentation assays, showing a shift to the supernatant in the pellet-to-supernatant ratios of TDP-43 (Figure 19H and I). Western blot results show no significant change in TDP-43 expression levels (Figure 19G).

A

B

C

D

E

F

G

H

I
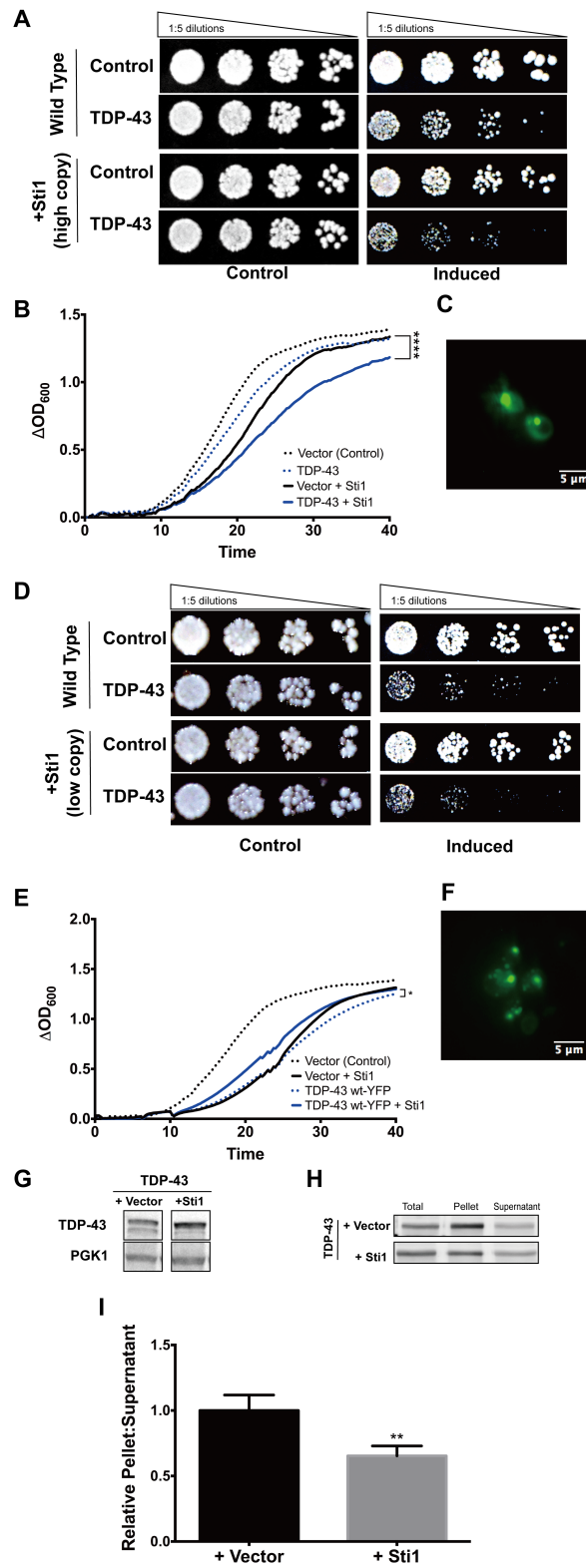
Figure 19: Sti1 and TDP-43 interaction in yeast – Sti1 overexpression. A Spotting assay of TDP-43-expressing wild type cells high copy overexpressing Sti1. **B** Growth curve assay of TDP-43-expressing wild type cells high copy overexpressing Sti1 with significance level p<0.0001. **C** Fluorescence microscopy TDP-43-expressing wild type cells high copy overexpressing Sti1. **D** Spotting assay of TDP-43-expressing wild type cells overexpressing low copy Sti1. **E** Growth curve assay of TDP-43-expressing wild type cells low copy overexpressing Sti1 with significance level p=0.05. **F** Fluorescence microscopy TDP-43-expressing wild type cells low copy overexpressing Sti1. **G** Western blots showing TDP-43 expression level of wild type cells low copy overexpressing Sti1. **H** Sedimentation assay of TDP-43-expressing wild type cells overexpressing low copy Sti1. **I** Statistical analysis of the sedimentation assay showing the change in TDP-43 pellet-to-supernatant ratio of cells overexpressing low copy Sti1 with significance level of p=0.01.

3.5 Mammalian Cells

We sought to validate the results shown for the overexpression of Sti1 in the TDP-43 yeast model in mammalian cells using HeLa, HEK, and N2a cells. The results are shown in the following sections.

3.5.1   HeLa Cells

We co-transfect TDP-43 and Sti1 into HeLa cells and perform a luciferase viability assay to assess the toxicity associated with TDP-43 and Sti1 expression on HeLa cells (Figure 20A). All constructs were transfected with an efficiency of more than 70%. TDP-43 shows no statistically different change in viability in HeLa cells. We also observe cell co-transfected with TDP-43, Sti1, and TDP-43 and Sti1 under the microscope using immunofluorescence (20C). TDP-43 is mostly localized in the nucleus and forms nuclear aggregates in HeLa cells, while Sti1 is diffusely localized in the cytoplasm. The sedimentation assays show no change in localization and aggregation of TDP43 when Sti1 is overexpressed (Figure 20B).
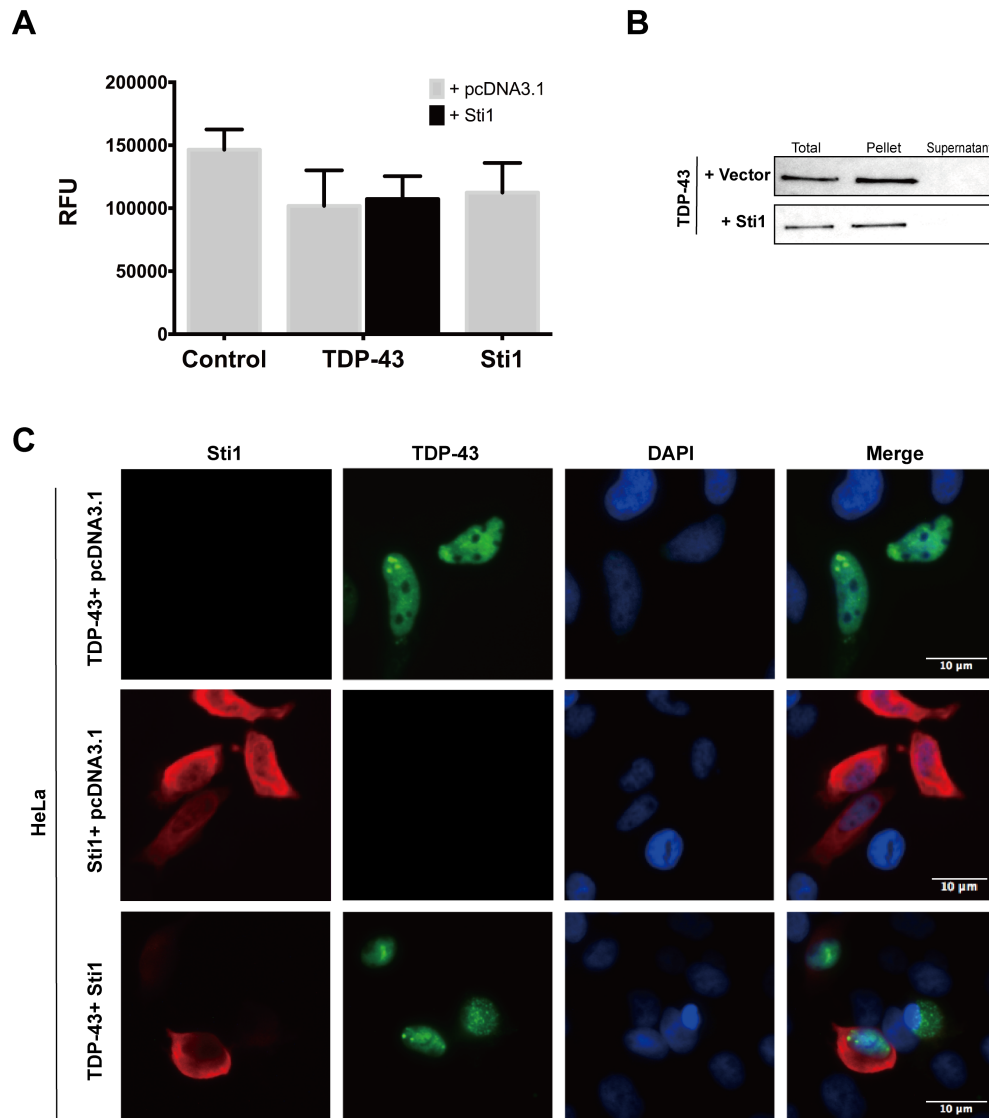
Figure 20: TDP-43 interaction with Sti1 in HeLa Cells. A Luciferase viability assay, **B** sedimentation assay, and **C** immunofluorescence microscopy of TDP-43 and Sti1 co-transfection.

3.5.2   HEK Cells

Due to the lack of TDP-43 aggregation and toxicity in HeLa cells, we utilize HEK wild type and Sti1 knock out (STI1KO) cells to study the interaction between TDP-43 and Sti1. The luciferase viability assay did not capture a change in toxicity between the different TDP-43 and Sti1 constructs as the transfection efficiency of HEK cells were low (only 30-40 %) (Figure 21A). Microscopy results in HEK wild type cells show cytoplasmic TDP-43 inclusions when TDP-43 is transfected with an empty pcDNA3.1 vector (Figure 21B), however TDP-43 localizes to the nucleus when cells express both the transfected Sti1 and TDP-43. HEK STI1KO cells do not show the same cytoplasmic TDP-43 inclusions as the wild type cells (Figure 21C).

A

B

C
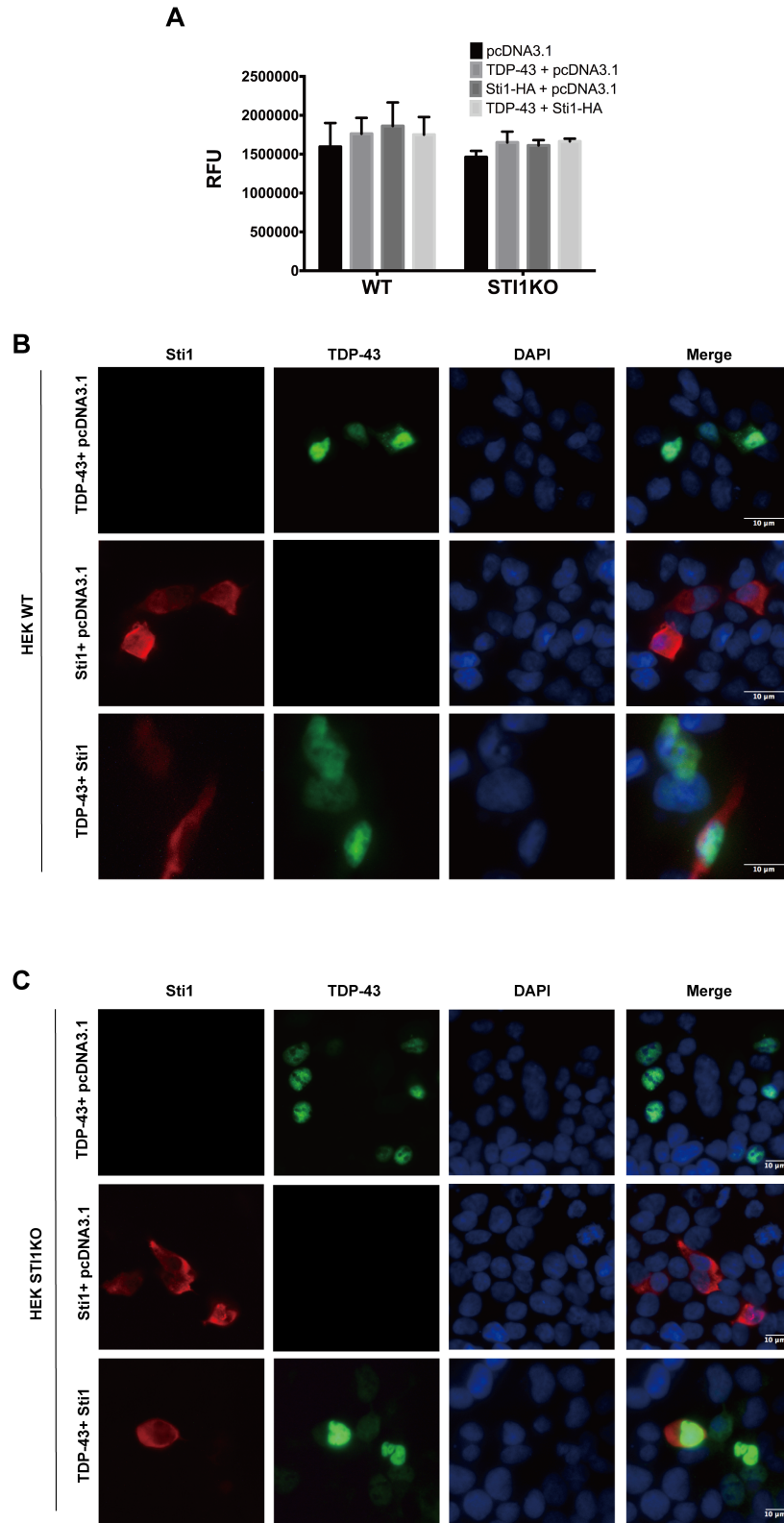
Figure 21: TDP-43 interaction with Sti1 in HEK WT and STI1KO Cells. A
Luciferase viability assay in HEK WT and STI1KO cells. B Immunofluorescence
microscopy in HEK WT, and **C** immunofluorescence microscopy in HEK STI1KO of
TDP-43 and Sti1 co-transfection.

3.5.3   N2a Cells

We utilize N2a cells to study the interaction between TDP-43 and Sti1, due to the lack of overall TDP-43 toxicity and mislocalization exhibited by the HEK and HeLa cells. TDP-43 exhibits significant toxicity in N2a cells, as shown in the luciferase viability assay (Figure 22A). We are able to see a significant rescue in toxicity when TDP-43 is co-expressed at a 2:1 (amount of DNA TDP-43-to-Sti1 used in transfection) ratio with Sti1 in N2a cells. When TDP-43 is co-expressed at different ratios with Sti1 (1:1 and 1:2), TDP-43 toxicity was not rescued.

Microscopy results in N2a cells show cytoplasmic TDP-43 localization when TDP-43 is transfected with an empty pcDNA3.1 vector (Figure 22B). We see a shift in TDP-43 localization when Sti1 is co-expressed at different levels. At a higher Sti1 co-expression level, TDP-43 is mostly localized in the nucleus, whereas at a lower Sti1 co-expression level, TDP-43 appears diffuse and is localized throughout the cell (Figure 22B).

These results demonstrate that N2a cells recapitulate major aspects of TDP-43 proteinopathy and toxicity. We thus conclude that N2a cells are optimal for our studies.
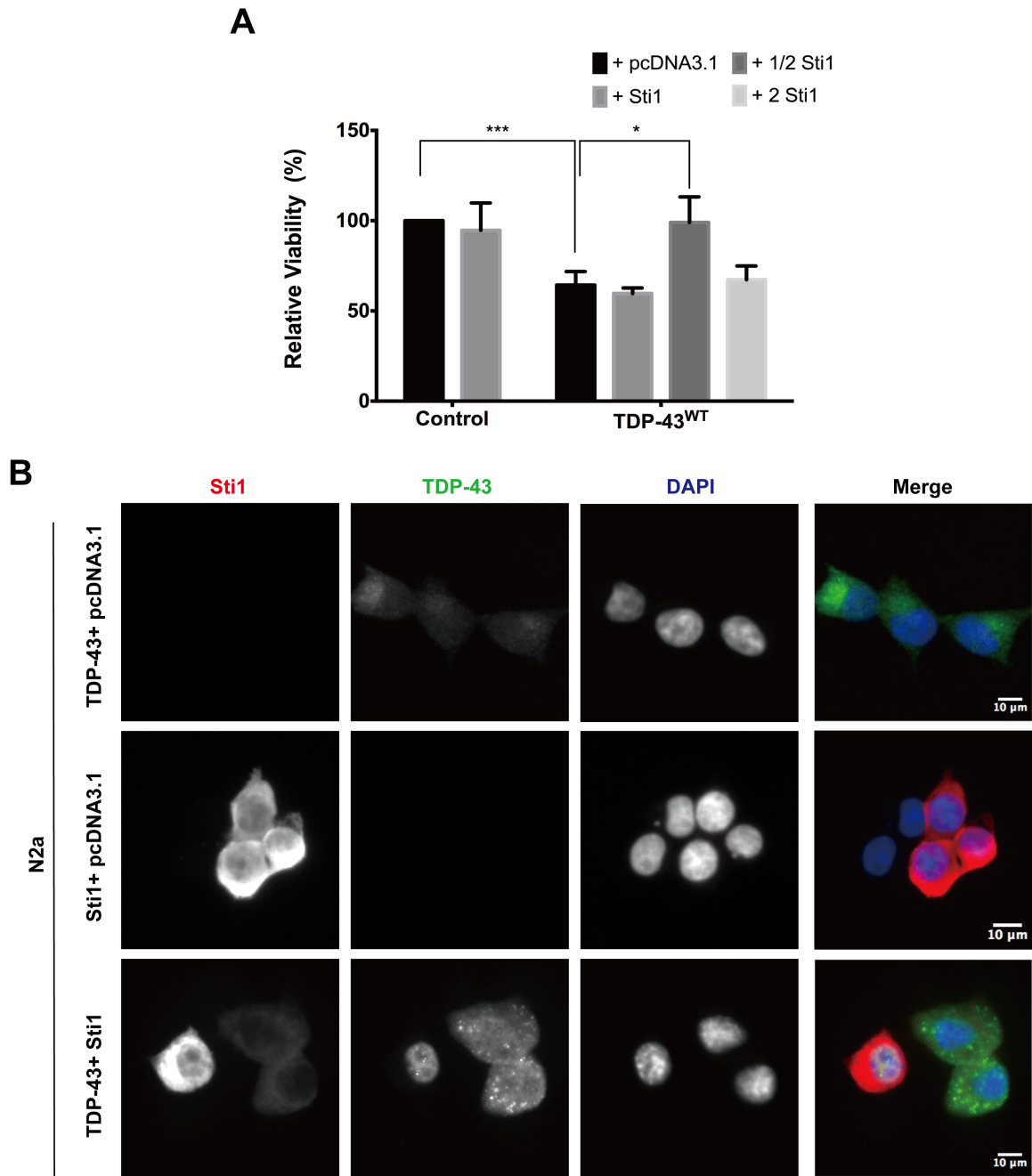
Figure 22: TDP-43 interaction with Sti1 in N2a Cells. A Luciferase viability assay in N2a cells with significance levels *** p<0.001 and * p<0.05. **B** Immunofluorescence microscopy in N2a of TDP-43 and Sti1 co-transfection.

Chapter 4

4   Discussion

4.1   Major Findings

4.1.1   Deletion of molecular chaperones

The effects of the deletion of Hsp90 and its co-chaperones on TDP-43 toxicity and aggregation in yeast are summarized in Table 4.

Table 4: Summarized results of the deletion of molecular chaperones.

Chaperones	Toxicity	Aggregation	TDP-43 Protein Level
Hsc82	No Change	No Change	No Change
Hsp82	No Change	No Change	No Change
Aha1	No Change	No Change	No Change
Cdc37	N/A	N/A	N/A
Sti1	**No Change**	**Reduced nuclear localization and increased cytosolic aggregation**	**No Change**

Although the deletion of these molecular chaperones do not show changes in toxicity, aggregation changes are seen in TDP-43 expressing *sti1Δ* cells. These cells have reduced nuclear TDP-43 localization and increased cytosolic aggregation compared to wild type cells expressing TDP-43. This suggests that the absence of Sti1 induces TDP-43 to exit the nucleus and form aggregates in the cytoplasm. This TDP-43 mislocalization could be the result of increased levels of aberrant TDP-43 species in the cell, inducing normal TDP-43 to misfold, and localize to the cytoplasm. It is plausible that upon exiting the nucleus, TDP-43 misfolds, forms aggregates, and induces the mislocalization and aggregation of further TDP-43 molecules. This notion is supported by previously published research [102], where TDP-43 found in ALS brains show prion-like properties, i.e. it seeds aggregation and propagates misfolding and aggregation intracellularly. TDP-

43 also shuttles forth and back between the cytoplasm and the nucleus as part of its normal function [67], providing an opportunity for contact with mislocalized and aggregated TDP-43 in the cytoplasm, and thus creating a feed forward cycle resulting in a rapid increase in toxic TDP-43 protein species that eventually leads to neuronal dysfunction and death.

The spotting assays performed with aged yeast cells show that *sti1Δ* cells expressing TDP-43 display increased toxicity compared to wild type and young control cells (Figure 18F and G). When observed under the microscope, these TDP-43 expressing *sti1Δ* cells (Figure 18H) show increased accumulation of soluble TDP-43 in the cytoplasm. This suggests that in order to combat toxicity associated with TDP-43 expression combined with the lack of Sti1 and the additional stress of aging, cells may have up-regulated other cellular protein quality control mechanisms to combat TDP-43 toxicity by breaking apart TDP-43 aggregates. However, breaking apart TDP-43 aggregates may instead create increased levels of highly toxic oligomeric TDP-43 protein species, thus exacerbating toxicity. While we need further experiments to support this interpretation, it is in line with recent research indicating that larger protein aggregates may be protective and that it is the soluble oligomeric species of a disease protein that is toxic [103].

4.1.2   Overexpression of Molecular Chaperones

The effect of the overexpression of molecular chaperones on TDP-43 toxicity and aggregation in yeast is summarized in Table 5 below.

Table 5: Summarized results of the overexpression of molecular chaperones.

Chaperones	Toxicity	Aggregation	TDP-43 Protein Level
Hsc82 (High copy)	Increase in toxicity****	No Change	Increased TDP-43 protein level***
Hsp82 (High copy)	Increase in toxicity****	No Change	Increased TDP-43 protein level**
Aha1 (High copy)	Increase in toxicity****	No Change	No Change
Cdc37 (High copy)	Increase in toxicity****	No Change	No Change
Sti1 (High copy)	**Increase in toxicity****	**Diffuse and no cytosolic aggregates**	**No Change**
Sti1 (Low copy)	**Rescue of toxicity ***	**Diffuse and soluble aggregates, sedimentation shows significant shift towards soluble TDP-43**	**No Change**

Asterisks indicate significance level: **** $p<0.0001$, *** $p<0.001$, ** $p<0.01$, * $p<0.05$.

In our experiments using overexpression of molecular chaperones, we observe a general increase in toxicity, even in the absence of TDP-43 expression. We conclude that "over-chaperoning" may be harmful to cells as the chaperones may possibly generate a toxic "gain-of-function" and interfere with existing protein quality control mechanisms. Also, the overexpression of Aha1, Cdc37, and Sti1, may lead to extensive inhibition of Hsp90, causing a toxic "loss-of-function" of Hsp90. However, it is also possible that this increase in toxicity is associated with an off-pathway mechanism.

In TDP-43 expressing cells, the overexpression of molecular chaperones may increase toxicity by creating or stabilizing highly toxic soluble oligomeric TDP-43 conformers. We can also infer from these results that the stoichiometric relationship between the amount of co-chaperones (Aha1, Cdc37, and Sti1), chaperones (Hsp90) and potential

substrates (TDP-43) present in the cell is important for optimal cellular protein quality control.

Notably, low copy overexpression of Sti1 shows a significant rescue of TDP-43 toxicity (Figure 19D) and shows a more diffuse TDP-43 localization profile that includes more soluble cytoplasmic protein (Figure 19F). Sedimentation assay results support the microscopy images and show a shift towards more soluble TDP-43 protein (Figure 19H and I). The changes in TDP-43 aggregation are unique to moderate overexpression of Sti1 and does not occur with overexpressed Hsc82, Hsp82, Aha1, and Cdc37, with Hsc82 and Hsp82 overexpression even increasing overall TDP-43 protein levels (Figure 14I and 15I) thus indicating a highly specific role in regulating TDP-43 aggregation, localization, and toxicity.

4.1.3   Mammalian cell work

We first utilized HeLa cells to study the changes in TDP-43 toxicity and aggregation in the presence of overexpressed Sti1. Notably TDP-43 toxicity in HeLa cells is not significant and thus cannot serve as a read out for TDP-43-Sti1 interactions. Microscopy results indicate nuclear localization of TDP-43 with some nuclear aggregates, which is distinct from TDP-43 expression in yeast cells (Figure 20B) and many other model organisms and cell systems (reviewed in [104]). We conclude that due to the persistent nuclear localization of TDP-43, HeLa cells may not be an ideal model to study TDP-43 proteinopathy as the mislocalization of TDP-43 from the nucleus into the cytoplasm is so central. It is plausible that the rapidly dividing HeLa cells dilute TDP-43 to such an extent that it remains in the nucleus and does not cause any measurable toxicity. Also, Sti1 is mostly localized to the cytoplasm in HeLa cells and hence cannot interact efficiently with nuclear TDP-43 aggregates (Figure 20C).

We next chose HEK cells to test the effects of co-expression of TDP-43 and Sti1 on TDP-43 aggregation and toxicity. Previous reports indicate some neuronal-like behavior in HEK cells [105] and they are consequently used in many studies on neurodegenerative diseases; however, HEK cells should by no means be regarded as proper neurons. We work with two HEK293 cell lines: wild type HEK cells and Sti1 knock out (STI1KO)

cells. The STI1KO HEK cells were engineered in the laboratory of our collaborator, Dr. Prado, at the Robarts Institute at Western University through CRISPR/Cas9 technology and generously shared with us for our TDP-43 experiments.

Viability assays of the two HEK cell lines do not show significant difference in the viability, i.e. TDP-43 toxicity (Figure 21A), which may be due to the low transfection efficiency in our HEK transfection protocol. Here, HEK cells adhere extremely poorly and therefore the transfection has been difficult and very inefficient. We are in the process of improving this experimental protocol. We therefore confine our interpretation of HEK cells on our immunofluorescence studies to shed light on the interaction between TDP-43 and Sti1. In wild type HEK cells (Figure 21B), TDP-43 localizes in both the nucleus and the cytoplasm and forms cytoplasmic inclusions, which is in good agreement with typical TDP-43 proteinopathy. On the other hand, STI1KO HEK cells show mostly nuclear TDP-43 localization (Figure 21C). Here, cells may have up regulated other protein quality control mechanisms to compensate for the lack of Sti1 in the cell, thus allowing TDP-43 to remain in the nucleus. We are currently characterizing the STI1KO HEK cell line to assess their expression of molecular chaperones and their cellular stress response programs.

Finally, we move into N2a cells to validate our key findings in a mammalian system. N2a cells are mouse neuroblastoma cells that are neuronal-like and can be further differentiated into cells that share similar properties to neurons [93]. These characteristics of N2a cells provide a good basis for conducting studies into neurodegenerative diseases. TDP-43 overexpression in N2a cells exhibits cytosolic mislocalization of TDP-43, a hallmark of TDP-43 proteinopathy, in addition to cellular toxicity, as shown in Fig 22. We are able to a rescue in TDP-43 toxicity when a moderate level of Sti1 is co-expressed with TDP-43 (Figure 22B), consistent with our findings in yeast. Our immunofluorescence results in N2a cells are also consistent with our yeast findings, where low-level co-expression of Sti1 results in a more diffuse TDP-43 localization profile that includes more soluble cytoplasmic protein, and higher levels of Sti1 result in a nuclear localization of TDP-43. On the whole, we find N2a cells a good model for TDP-43 proteinopathy and we are able to validate our key findings in N2a cells.

4.2 A new sedimentation assay to quantitatively determine changes in protein aggregation

TDP-43 aggregation and solubility are documented properly by our newly developed sedimentation assay. Yet the characterization of endogenous molecular chaperones that associated with misfolded and aggregated protein under cellular stress conditions using the same sedimentation assay did not produce conclusive results. As shown in Figure 13, endogenous molecular chaperones (e.g. Hsp70 and Hsp90) are rather abundant in all eukaryotic cells and therefore relative changes in solubility under stress conditions are difficult to document.

Overall the sedimentation assay documents changes in aggregation patterns of aggregating or misfolding proteins, such as TDP-43 (Figure 12) and alpha-synuclein (data not shown) in both yeast cells and mammalian cells. Notably, the quantitative assessment of the aggregation of these two neurodegenerative disease proteins has been challenging using standard biochemical assays. Also, our sedimentation protocol is very close to standard protein lysis and SDS-PAGE protocols, and is accordingly much easier to implement than traditional means of detection, e.g. by subcellular fractionation using sucrose cushions or comparable methods.

4.3 Hsp90 stabilization of aberrant TDP-43 protein species leads to cellular toxicity

Previous studies on tau aggregation in AD have found that Hsp90 stabilizes the aberrant form of tau and contributes to the accumulation of these toxic protein species in the cell [9]. Hsp90 inhibition has accordingly been proposed as a potential therapeutic target of tauopathies and may even prove to be beneficial for other neurodegenerative diseases associated with protein misfolding [29].

Our findings are in line with this point of view. We observe an increase in TDP-43 protein levels (Figure 14 and 15 H, I) and an increase in toxicity of TDP-43 when Hsp90 is overexpressed (Fig 14 and 15 D and E). The higher TDP-43 protein level in these constructs may be due to the stabilization of TDP-43 by Hsp90 due to a direct interaction

between TDP-43 and Hsp90 leading to cellular toxicity through the accumulation of toxic TDP-43 species in the cell.

4.4 Moderate expression of Sti1 reduces TDP-43 toxicity through changes in its localization and aggregation

Our results indicate that reduced TDP-43 toxicity through moderate overexpression of Sti1 is directly linked to the change in TDP-43 localization and aggregation. This is may be due to Sti1's role as an Hsp90 inhibitor. As discussed in section 4.3, Hsp90 may stabilize aberrant forms of TDP-43 and lead to an accumulation of toxic TDP-43 species in the cell. Through the inhibition of Hsp90 by Sti1, other molecular chaperones such as the Hsp70 chaperoning complex are allowed to take its place and direct TDP-43 aggregates to be degraded through UPS or dissolved by dissaggregases such as Hsp104 in yeast [100] or Hsp70 and Hsp110 in mammalian cells [106]. Also, strong overexpression of Sti1 shows reduced levels of cytoplasmic TDP-43. High expression levels of Sti1 may strongly inhibit Hsp90 activity, leading to a toxic "loss-of-function" as well as a toxic "gain-of-function" due to the abundance of Sti1 as discussed above in section 4.1.2. On the other hand, the lack of Sti1 can also result in toxicity in the cell. The role of Sti1 in keeping TDP-43 localized to the nucleus and decreasing the amount of cytoplasmic TDP-43 is confirmed in our results using N2a cells. Cells expressing TDP-43 and high-levels of Sti1 show almost exclusive nuclear localization of TDP-43, whereas the majority of cells that express TDP-43 and only endogenous level of Sti1 show mostly cytoplasmic localization of Sti1.

Our results also indicate that TDP-43 nuclear localization is impaired in *sti1Δ* cells, leading to more cytoplasmic TDP-43 and increased cellular toxicity, which is exacerbated in aged *sti1Δ* cells. Here, TDP-43 accumulates in the cytoplasm over time, increasing its cellular toxicity. Aberrant TDP-43 species can also provide a template for TDP-43 to misfold and form larger aggregates when associated with cytoplasmic TDP-43, causing more TDP-43 to mislocalize and accumulate in the cytoplasm as discussed as a possible prion-like mechanism in section 4.1.1. Consequently, only moderate Sti1 overexpression proves to be beneficial in cells that express TDP-43.

The proposed mechanism of TDP-43/Sti1 interactions is illustrated in Figure 22 below. While further experiments are required to decipher the precise cellular and molecular underpinnings, all these different proposed mechanisms support our hypothesis, that **Sti1 specifically rescues TDP-43 toxicity and modifies its aggregation patterns**.

A
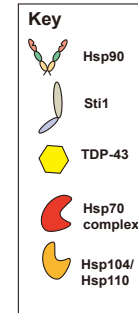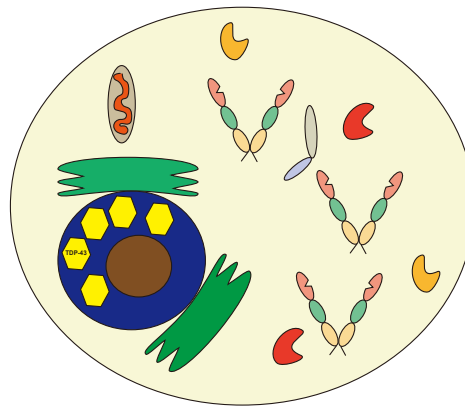
Under normal conditions, TDP-43 is localized in the nucleus
and does not interact with cytoplasmic Hsp90 or Sti1.

B

Limited Sti1 inhibition of Hsp90

Hsp90 binds and
stabilizes TDP-43
resulting in the
accumulation of
TDP-43 and increased
cellular toxicity

Normal TDP-43
forms aggregates
with aberrant TDP-43
and cannot be shuttled back
into the nucleus
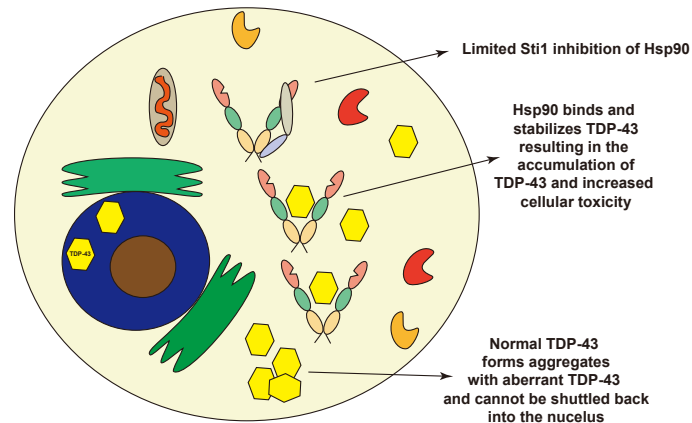
TDP-43 proteinopathy, TDP-43 is mislocalized to the cytoplasm and forms aggregates.

C

Moderate Sti1 inhibition of Hsp90

Less aberrant
TDP-43 species
in cytoplasm,
allowing normal
TDP-43 to be shuttled
back into the nucleus

Aberrant TDP-43 species
tagged for degredation
through UPS by
other chaperones
i.e. Hsp70 complex

TDP-43 aggregates broken apart
by chaperones i.e. Hsp104 or Hsp110
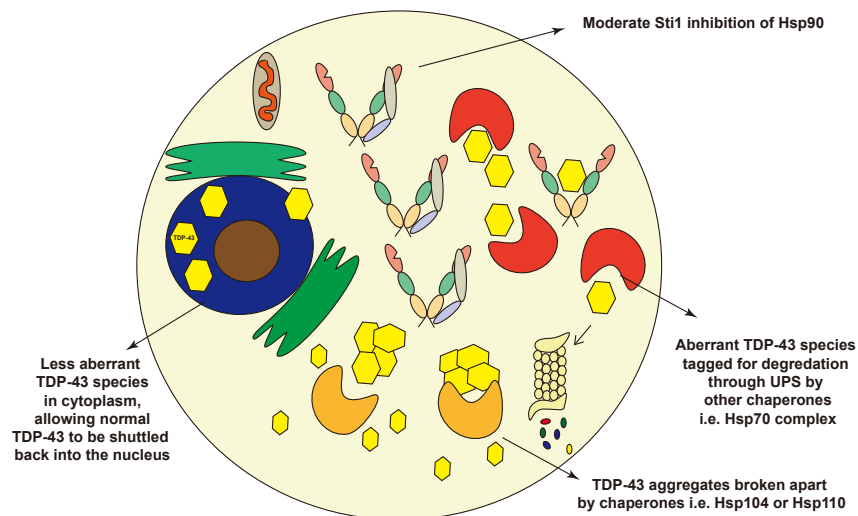
The moderate up regulation of Sti1 can inhibit Hsp90 activity and the binding to TDP-43.
Through the inhibition of Hsp90, other molecular chaperones can interact with TDP-43, reducing toxicity

Key

Hsp90

Sti1

TDP-43

Hsp70
complex

Hsp104/
Hsp110

Figure 23: Proposed mechanisms for the interaction between Sti1 and TDP-43. A Under normal conditions, TDP-43 and Sti1 localize to different cellular compartments and do not interact. **B** In TDP-43 proteinopathy, TDP-43 is mislocalized to the cytoplasm, allowing Sti1 and TDP-43 to interact. **C** When Sti1 is moderately overexpressed in TDP-43 proteinopathy, cellular toxicity is reduced by Sti1's role as Hsp90 inhibitor, allowing other molecular chaperones to interact and more effectively degrade or break apart TDP-43 aggregation.

4.5 Conclusion

Our study provides evidence that Sti1 can rescue TDP-43 toxicity by modifying its aggregation pattern in a dose-dependent manner. We propose that **Hsp90 stabilizes toxic TDP-43 species in TDP-43 proteinopathy, leading to an accumulation of TDP-43 in the cytoplasm and cellular toxicity. Moderate overexpression of Sti1 can correct this process by inhibiting Hsp90, allowing other molecular chaperones to break apart aggregates or direct toxic TDP-43 species to be degraded by UPS.**

Importantly, it is also possible that Sti1 interacts directly with TDP-43. Recent studies have shown Sti1 to be involved in many cellular processes outside of the Hsp90 and Hsp70 chaperoning complex [43]; therefore, it is possible that Sti1 may interact with TDP-43 independent of Hsp90, but further studies need to be done to confirm this theory.

4.6 Limitations

Yeast models are powerful model systems to study basic mechanisms of cellular protein quality control and its interaction with misfolded proteins associated with neurodegenerative disease. The conservation of key cellular pathways between yeast and humans, such as the ones regulating cellular protein quality control, makes experiments in yeast directly relevant to human and can be used to decipher aspects of the pathogeneses of neurodegenerative diseases. Such is the case in our study.

The yeast model system has its limitations. Unlike humans, yeast is a unicellular organism that does not have differentiated cell types, such as the motor neurons affected in ALS, to faithfully recapitulate interactions between different cell types of high-level organisms.

We replicate our key findings in yeast in a mammalian model system using HEK, HeLa, and N2a cells to relate back to human neurodegenerative disease and ALS pathology. ALS is a neurodegenerative disease that occurs predominantly in motor neurons. HEK cells share some features with immature neuronal cells, but it is not truly a neuronal cell

line and may behave differently than neurons in many regards, including sensitivity to TDP-43 misfolding. Although we are able to utilize differentiated N2a cells to model TDP-43 and Sti1 interaction in neuronal-like cells, N2a cells contain endogenous copies of mouse TDP-43 that may behave differently compared to human TDP-43. In order to apply our findings to TDP-43 proteinopathy and ALS pathology, studies in primary neuron cells or even transgenic mouse models need to be conducted in the future. Primary neuronal cell lines can provide more insight to the loss-of-function aspects associated with the death of motor neurons in ALS, while mouse models can provide a systematic insight into cell-type and tissue-specific aspects of ALS pathogenesis.

Though the model systems used in our study have limitations, they help to elucidate the basic mechanistic framework underlying TDP-43 proteinopathy and have the potential to initiate the identification of previously unexplored therapeutic targets for ALS.

4.7 Future work

The interaction between Sti1 and TDP-43 documented by our findings provides novel insight into how TDP-43 proteinopathy can be corrected by targeting Sti1. However, several questions remain unanswered and need to be addressed to confirm our theory.

We speculate that Sti1 interacts indirectly with TDP-43 through Hsp90, and it is the inhibition of Hsp90 through Sti1 that rescues TDP-43 toxicity. In experiments performed by our collaborators in Dr. Prado's Lab at the Robarts Institute, Western University, TDP-43 was found to co-immunoprecipitate with Sti1. This suggests a direct interaction between Sti1 and TDP-43. Whether Sti1 interacts with TDP-43 directly or indirectly through Hsp90 will have to be tested through experiments involving Hsp90 deletion in yeast or knock out models in mammalian cells in future experiments.

The Sti1KO HEK cell line used in this study is a novel cell line that has not been characterized in the literature. The overexpression results of TDP-43 in these Sti1KO cells show that TDP-43 localizes to the nucleus in this model, which is not consistent with the yeast results obtained through expression of TDP-43 in Sti1 deletion cells. HEK cells are cancer-derived cells that are highly genetically mutated and do not fully

represent physiological conditions in normal cells. In order to interpret our results in this cell line, further characterization of these cells, including the endogenous expression level of other molecular chaperones and their response to stress conditions, are required.

Our studies focused on the localization of TDP-43 and Sti1 transfected in HeLa, HEK, and N2a cells. The localization and expression of endogenous TDP-43 and Sti1 is experimentally challenging because of low endogenous protein levels and were therefore not yet examined. These experiments should also be performed to fully understand the interaction between these two proteins at endogenous expression levels.

As mentioned in the limitations (section 4.5), our model systems do not capture the effect of Sti1 over-expression on TDP-43 in neurons. The results in our study should be replicated in neuronal (e.g. primary cells) in order to apply our proposed mechanism to motor neurons of ALS. In addition to experiments in cell culture, TDP-43 mouse models should be adopted to understand the systematic effects of targeting Sti1 to correct TDP-43 proteinopathy.

Aging is an important factor in ALS, as well as many other neurodegenerative diseases involving TDP-43 proteinopathy or protein misfolding generally. The effect of aging on the "loss-of-function" of molecular chaperones, specifically Sti1, and how this influences TDP-43 to mislocalize and aggregate needs to be further studied. Though this study demonstrated increased TDP-43 toxicity in aged yeast cells lacking Sti1, the full effect of aging and the cellular protein quality control mechanisms in response to aging should be addressed in greater detail.

The function of Sti1 outside of its role as Hsp90 co-chaperone is not as well established. While our results suggest that Sti1 genetically interacts with TDP-43 through the inhibition of Hsp90, it is plausible that Sti1 directly interacts with TDP-43. Further studies into this subject matter may shed light on the interaction between TDP-43 and Sti1. For instance, the interaction between Sti1 and TDP-43 can be understood more in depth through biochemical analysis using the purified proteins. Through the interaction of the purified proteins of TDP-43 and Sti1, the underlying molecular mechanism can be surmised.

4.8 Significance

The specific interaction between TDP-43 and Sti1 described in this study is a novel finding and encourages further detailed mechanistic and pathological studies.

ALS mainly manifests at a later onset, therefore aging is an important factor in the disease. This study shows an interaction between Sti1 and TDP-43 in chaperoning the mislocalization and aggregation of TDP-43. Further studies may be able to establish whether Sti1 loss-of-function due to aging is important in the mislocalization and accumulation of toxic species of TDP-43, leading to TDP-43 proteinopathy.

TDP-43 proteinopathy is important in the pathogenesis of ALS, as well as other neurodegenerative diseases, such as FTD, AD, PD, and HD. This study begins to decipher genetic and molecular mechanisms by which targeting of TDP-43 by Hsp90 in an attempt to correct its mislocalization and accumulation of TDP-43 leads to TDP-43 proteinopathy. This might eventually help to establish Hsp90 and its co-chaperones Sti1 specifically as a selective therapeutic target to remedy TDP-43 proteinopathy in ALS and other neurodegenerative diseases.

References

1. Scotter, E.L., H.-J. Chen, and C.E. Shaw, *TDP-43 Proteinopathy and ALS: Insights into Disease Mechanisms and Therapeutic Targets.* Neurotherapeutics, 2015. **12**(2): p. 352-363.

2. Ross, C.A. and M.A. Poirier, *Opinion: What is the role of protein aggregation in neurodegeneration?* Nat Rev Mol Cell Biol, 2005. **6**(11): p. 891-8.

3. Ellis, R.J. and S.M. van der Vies, *Molecular chaperones.* Annu Rev Biochem, 1991. **60**: p. 321-47.

4. Lindberg, I., et al., *Chaperones in Neurodegeneration.* Journal of Neuroscience, 2015. **35**(41): p. 13853-13859.

5. Ojha, J., et al., *Sequestration of Toxic Oligomers by HspB1 as a Cytoprotective Mechanism.* Molecular and Cellular Biology, 2011. **31**(15): p. 3146-3157.

6. Zhao, R. and W.A. Houry, *Hsp90: a chaperone for protein folding and gene regulation.* Biochem Cell Biol, 2005. **83**(6): p. 703-10.

7. Borkovich, K.A., et al., *hsp82 is an essential protein that is required in higher concentrations for growth of cells at higher temperatures.* Molecular and Cellular Biology, 1989. **9**(9): p. 3919-3930.

8. Zuehlke, A., J.L. Johnson, and J.E. Gestwicki, *Hsp90 and co-chaperones twist the functions of diverse client proteins.* Biopolymers, 2010. **93**(3): p. 211-217.

9. Luo, W., et al., *Heat shock protein 90 in neurodegenerative diseases.* Mol Neurodegener, 2010. **5**: p. 24.

10. Luo, W., A. Rodina, and G. Chiosis, *Heat shock protein 90: translation from cancer to Alzheimer's disease treatment?* BMC Neurosci, 2008. **9 Suppl 2**: p. S7.

11. Johnson, B.S., et al., *A yeast TDP-43 proteinopathy model: Exploring the molecular determinants of TDP-43 aggregation and cellular toxicity.* Proc Natl Acad Sci U S A, 2008. **105**(17): p. 6439-44.

12. Verghese, J., et al., *Biology of the heat shock response and protein chaperones: budding yeast (Saccharomyces cerevisiae) as a model system.* Microbiol Mol Biol Rev, 2012. **76**(2): p. 115-58.

13. Mohammadi, S., et al., *On the scope and limitations of baker's yeast as a model organism for studying human tissue-specific pathways.* 2014.

14. Chen, B., et al., *Cellular strategies of protein quality control.* Cold Spring Harb Perspect Biol, 2011. **3**(8): p. a004374.

15. Dobson, C.M., *Protein folding and misfolding.* Nature, 2003. **426**(6968): p. 884-90.

16. Hartl, F.U. and M. Hayer-Hartl, *Molecular chaperones in the cytosol: from nascent chain to folded protein.* Science, 2002. **295**(5561): p. 1852-8.

17. Muchowski, P.J. and J.L. Wacker, *Modulation of neurodegeneration by molecular chaperones.* Nat Rev Neurosci, 2005. **6**(1): p. 11-22.

18. Tyedmers, J., A. Mogk, and B. Bukau, *Cellular strategies for controlling protein aggregation.* Nat Rev Mol Cell Biol, 2010. **11**(11): p. 777-88.

19. Voisine, C., J.S. Pedersen, and R.I. Morimoto, *Chaperone networks: tipping the balance in protein folding diseases.* Neurobiol Dis, 2010. **40**(1): p. 12-20.

20. Li, J., J. Soroka, and J. Buchner, *The Hsp90 chaperone machinery: conformational dynamics and regulation by co-chaperones.* Biochim Biophys Acta, 2012. **1823**(3): p. 624-35.

21. Jackson, S.E., *Hsp90: Structure and Function.* 2012. **328**: p. 155-240.

22. Terasawa, K., M. Minami, and Y. Minami, *Constantly updated knowledge of Hsp90.* J Biochem, 2005. **137**(4): p. 443-7.

23. Wayne, N. and D.N. Bolon, *Dimerization of Hsp90 is required for in vivo function. Design and analysis of monomers and dimers.* J Biol Chem, 2007. **282**(48): p. 35386-95.

24. Prodromou, C., et al., *The ATPase cycle of Hsp90 drives a molecular 'clamp' via transient dimerization of the N-terminal domains.* EMBO J, 2000. **19**(16): p. 4383-92.

25. Panaretou, B., et al., *Activation of the ATPase Activity of Hsp90 by the Stress-Regulated Cochaperone Aha1.* Molecular Cell, 2002. **10**(6): p. 1307-1318.

26. Rehn, A.B. and J. Buchner, *p23 and Aha1.* Subcell Biochem, 2015. **78**: p. 113-31.

27. Wayne, N. and D.N. Bolon, *Charge-rich regions modulate the anti-aggregation activity of Hsp90.* J Mol Biol, 2010. **401**(5): p. 931-9.

28. Evans, C.G., S. Wisen, and J.E. Gestwicki, *Heat shock proteins 70 and 90 inhibit early stages of amyloid beta-(1-42) aggregation in vitro.* J Biol Chem, 2006. **281**(44): p. 33182-91.

29. Garcia-Carbonero, R., A. Carnero, and L. Paz-Ares, *Inhibition of HSP90 molecular chaperones: moving into the clinic.* The Lancet Oncology, 2013. **14**(9): p. e358-e369.

30. Shiau, A.K., et al., *Structural Analysis of E. coli hsp90 reveals dramatic nucleotide-dependent conformational rearrangements.* Cell, 2006. **127**(2): p. 329-40.

31. Lotz, G.P., et al., *Aha1 binds to the middle domain of Hsp90, contributes to client protein activation, and stimulates the ATPase activity of the molecular chaperone.* J Biol Chem, 2003. **278**(19): p. 17228-35.

32. Harst, A., H. Lin, and W.M. Obermann, *Aha1 competes with Hop, p50 and p23 for binding to the molecular chaperone Hsp90 and contributes to kinase and hormone receptor activation.* Biochem J, 2005. **387**(Pt 3): p. 789-96.

33. Retzlaff, M., et al., *Asymmetric activation of the hsp90 dimer by its cochaperone aha1.* Mol Cell, 2010. **37**(3): p. 344-54.

34. Tripathi, V., et al., *Aha1 can act as an autonomous chaperone to prevent aggregation of stressed proteins.* J Biol Chem, 2014. **289**(52): p. 36220-8.

35. Tochio, N., Koshiba, S., Inoue, M., Kigawa, T., Yokoyama, S., *The solution structure of the C-terminal domain of human Activator of 90 kDa heat shock protein ATPase homolog 1.* 2005.

36. Reed, S.I., *The selection of amber mutations in genes required for completion of start, the controlling event of the cell division cycle of S. cerevisiae.* Genetics, 1980. **95**(3): p. 579-88.

37. Gray, P.J., Jr., et al., *Targeting the oncogene and kinome chaperone CDC37.* Nat Rev Cancer, 2008. **8**(7): p. 491-5.

38. Calderwood, S.K., *Cdc37 as a co-chaperone to Hsp90.* Subcell Biochem, 2015. **78**: p. 103-12.

39. Roe, S.M., et al., *The Mechanism of Hsp90 Regulation by the Protein Kinase-Specific Cochaperone p50cdc37.* Cell, 2004. **116**(1): p. 87-98.

40. Kimura, Y., et al., *Cdc37 is a molecular chaperone with specific functions in signal transduction.* Genes & Development, 1997. **11**(14): p. 1775-1785.

41. Sreeramulu, S., et al., *The human Cdc37.Hsp90 complex studied by heteronuclear NMR spectroscopy.* J Biol Chem, 2009. **284**(6): p. 3885-96.

42. Nicolet, C.M. and E.A. Craig, *Isolation and characterization of STI1, a stress-inducible gene from Saccharomyces cerevisiae.* Mol Cell Biol, 1989. **9**(9): p. 3638-46.

43. Odunuga, O.O., V.M. Longshaw, and G.L. Blatch, *Hop: more than an Hsp70/Hsp90 adaptor protein.* Bioessays, 2004. **26**(10): p. 1058-68.

44. Kryndushkin, D.S., et al., *Increased expression of Hsp40 chaperones, transcriptional factors, and ribosomal protein Rpp0 can cure yeast prions.* J Biol Chem, 2002. **277**(26): p. 23702-8.

45. Prodromou, C., *The 'active life' of Hsp90 complexes.* Biochim Biophys Acta, 2012. **1823**(3): p. 614-23.

46. Soti, C. and P. Csermely, *Molecular chaperones and the aging process.* Biogerontology, 2000. **1**(3): p. 225-33.

47. Shamovsky, I. and E. Nudler, *New insights into the mechanism of heat shock response activation.* Cell Mol Life Sci, 2008. **65**(6): p. 855-61.

48. Zou, J., et al., *Repression of Heat Shock Transcription Factor HSF1 Activation by HSP90 (HSP90 Complex) that Forms a Stress-Sensitive Complex with HSF1.* Cell, 1998. **94**(4): p. 471-480.

49. Kiernan, M.C., et al., *Amyotrophic lateral sclerosis.* Lancet, 2011. **377**(9769): p. 942-55.

50. Ju, S., et al., *A yeast model of FUS/TLS-dependent cytotoxicity.* PLoS Biol, 2011. **9**(4): p. e1001052.

51. Lagier-Tourenne, C. and D.W. Cleveland, *Rethinking ALS: the FUS about TDP-43.* Cell, 2009. **136**(6): p. 1001-4.

52. Blokhuis, A.M., et al., *Protein aggregation in amyotrophic lateral sclerosis.* Acta Neuropathol, 2013. **125**(6): p. 777-94.

53. Rosen, D.R., et al., *Mutations in Cu/Zn superoxide dismutase gene are associated with familial amyotrophic lateral sclerosis.* Nature, 1993. **362**(6415): p. 59-62.

54. Bastow, E.L., C.W. Gourlay, and M.F. Tuite, *Using yeast models to probe the molecular basis of amyotrophic lateral sclerosis.* Biochem Soc Trans, 2011. **39**(5): p. 1482-7.

55. Grad, L.I., et al., *Intermolecular transmission of superoxide dismutase 1 misfolding in living cells.* Proc Natl Acad Sci U S A, 2011. **108**(39): p. 16398-403.

56. Grad, L.I., et al., *Exosome-dependent and independent mechanisms are involved in prion-like transmission of propagated Cu/Zn superoxide dismutase misfolding.* Prion, 2014. **8**(5): p. 331-5.

57. Neumann, M., et al., *Ubiquitinated TDP-43 in frontotemporal lobar degeneration and amyotrophic lateral sclerosis.* Science, 2006. **314**(5796): p. 130-3.

58. van den Heuvel, D.M., et al., *Taking a risk: a therapeutic focus on ataxin-2 in amyotrophic lateral sclerosis?* Trends Mol Med, 2014. **20**(1): p. 25-35.

59. Kwiatkowski, T.J., Jr., et al., *Mutations in the FUS/TLS gene on chromosome 16 cause familial amyotrophic lateral sclerosis.* Science, 2009. **323**(5918): p. 1205-8.

60. DeJesus-Hernandez, M., et al., *Expanded GGGGCC hexanucleotide repeat in noncoding region of C9ORF72 causes chromosome 9p-linked FTD and ALS.* Neuron, 2011. **72**(2): p. 245-56.

61. Keller, B.A., et al., *Co-aggregation of RNA binding proteins in ALS spinal motor neurons: evidence of a common pathogenic mechanism.* Acta Neuropathol, 2012. **124**(5): p. 733-47.

62. Kenna, K.P., et al., *NEK1 variants confer susceptibility to amyotrophic lateral sclerosis.* Nat Genet, 2016. **48**(9): p. 1037-42.

63. Droppelmann, C.A., et al., *Rho guanine nucleotide exchange factor is an NFL mRNA destabilizing factor that forms cytoplasmic inclusions in amyotrophic lateral sclerosis.* Neurobiol Aging, 2013. **34**(1): p. 248-62.

64. Li, H.F. and Z.Y. Wu, *Genotype-phenotype correlations of amyotrophic lateral sclerosis.* Transl Neurodegener, 2016. **5**: p. 3.

65. Ling, J.P., et al., *TDP-43 repression of nonconserved cryptic exons is compromised in ALS-FTD.* Science, 2015. **349**(6248): p. 650-5.

66. Vanden Broeck, L., P. Callaerts, and B. Dermaut, *TDP-43-mediated neurodegeneration: towards a loss-of-function hypothesis?* Trends Mol Med, 2014. **20**(2): p. 66-71.

67. Ayala, Y.M., et al., *Structural determinants of the cellular localization and shuttling of TDP-43.* J Cell Sci, 2008. **121**(Pt 22): p. 3778-85.

68. Mackenzie, I.R.A., R. Rademakers, and M. Neumann, *TDP-43 and FUS in amyotrophic lateral sclerosis and frontotemporal dementia.* The Lancet Neurology, 2010. **9**(10): p. 995-1007.

69. Dormann, D. and C. Haass, *TDP-43 and FUS: a nuclear affair.* Trends Neurosci, 2011. **34**(7): p. 339-48.

70. Ou, S.H., et al., *Cloning and characterization of a novel cellular protein, TDP-43, that binds to human immunodeficiency virus type 1 TAR DNA sequence motifs.* J Virol, 1995. **69**(6): p. 3584-96.

71. Nehls, J., et al., *HIV-1 replication in human immune cells is independent of TAR DNA binding protein 43 (TDP-43) expression.* PLoS One, 2014. **9**(8): p. e105478.

72.   Chen-Plotkin, A.S., V.M. Lee, and J.Q. Trojanowski, *TAR DNA-binding protein 43 in neurodegenerative disease.* Nat Rev Neurol, 2010. **6**(4): p. 211-20.

73.   Swinnen, B. and W. Robberecht, *The phenotypic variability of amyotrophic lateral sclerosis.* Nat Rev Neurol, 2014. **10**(11): p. 661-70.

74.   Rohn, T.T., *Caspase-cleaved TAR DNA-binding protein-43 is a major pathological finding in Alzheimer's disease.* Brain Res, 2008. **1228**: p. 189-98.

75.   Chanson, J.B., et al., *TDP43-positive intraneuronal inclusions in a patient with motor neuron disease and Parkinson's disease.* Neurodegener Dis, 2010. **7**(4): p. 260-4.

76.   Rayaprolu, S., et al., *TARDBP mutations in Parkinson's disease.* Parkinsonism Relat Disord, 2013. **19**(3): p. 312-5.

77.   Fuentealba, R.A., et al., *Interaction with polyglutamine aggregates reveals a Q/N-rich domain in TDP-43.* J Biol Chem, 2010. **285**(34): p. 26304-14.

78.   Chiang, C.H., et al., *Structural analysis of disease-related TDP-43 D169G mutation: linking enhanced stability and caspase cleavage efficiency to protein accumulation.* Sci Rep, 2016. **6**: p. 21581.

79.   Johnson, B.S., et al., *TDP-43 is intrinsically aggregation-prone, and amyotrophic lateral sclerosis-linked mutations accelerate aggregation and increase toxicity.* J Biol Chem, 2009. **284**(30): p. 20329-39.

80.   Pokrishevsky, E., et al., *Aberrant localization of FUS and TDP43 is associated with misfolding of SOD1 in amyotrophic lateral sclerosis.* PLoS One, 2012. **7**(4): p. e35050.

81.   Pokrishevsky, E., L.I. Grad, and N.R. Cashman, *TDP-43 or FUS-induced misfolded human wild-type SOD1 can propagate intercellularly in a prion-like fashion.* Sci Rep, 2016. **6**: p. 22155.

82.   Braun, R.J., et al., *Nervous yeast: modeling neurotoxic cell death.* Trends Biochem Sci, 2010. **35**(3): p. 135-44.

83.   Pereira, C., et al., *A yeast model of the Parkinson's disease-associated protein Parkin.* Exp Cell Res, 2015. **333**(1): p. 73-9.

84.   Outeiro, T.F. and S. Lindquist, *Yeast cells provide insight into alpha-synuclein biology and pathobiology.* Science, 2003. **302**(5651): p. 1772-5.

85.   Duennwald, M.L., *Polyglutamine misfolding in yeast: toxic and protective aggregation.* Prion, 2011. **5**(4): p. 285-90.

86.   Bharadwaj, P., R. Martins, and I. Macreadie, *Yeast as a model for studying Alzheimer's disease.* FEMS Yeast Res, 2010. **10**(8): p. 961-9.

87.   Chafekar, S.M., et al., *Pharmacological tuning of heat shock protein 70 modulates polyglutamine toxicity and aggregation.* ACS Chem Biol, 2012. **7**(9): p. 1556-64.

88.   Eisenberg, T., et al., *The mitochondrial pathway in yeast apoptosis.* Apoptosis, 2007. **12**(5): p. 1011-23.

89.   Armakola, M., M.P. Hart, and A.D. Gitler, *TDP-43 toxicity in yeast.* Methods, 2011. **53**(3): p. 238-45.

90.   Katzen, F., *Gateway((R)) recombinational cloning: a biological operating system.* Expert Opin Drug Discov, 2007. **2**(4): p. 571-89.

91.   Romanos, M.A., C.A. Scorer, and J.J. Clare, *Foreign gene expression in yeast: a review.* Yeast, 1992. **8**(6): p. 423-88.

92.   Chafekar, S.M. and M.L. Duennwald, *Impaired heat shock response in cells expressing full-length polyglutamine-expanded huntingtin.* PLoS One, 2012. **7**(5): p. e37929.

93.   Tremblay, R.G., et al., *Differentiation of mouse Neuro 2A cells into dopamine neurons.* J Neurosci Methods, 2010. **186**(1): p. 60-7.

94.   Summers, D.W. and D.M. Cyr, *Use of yeast as a system to study amyloid toxicity.* Methods, 2011. **53**(3): p. 226-31.

95.   Theodoraki, M.A., et al., *A network of ubiquitin ligases is important for the dynamics of misfolded protein aggregates in yeast.* J Biol Chem, 2012. **287**(28): p. 23911-22.

96.   Shiber, A., et al., *Ubiquitin conjugation triggers misfolded protein sequestration into quality control foci when Hsp70 chaperone levels are limiting.* Mol Biol Cell, 2013. **24**(13): p. 2076-87.

97.   Trotter, E.W., et al., *Misfolded proteins are competent to mediate a subset of the responses to heat shock in Saccharomyces cerevisiae.* J Biol Chem, 2002. **277**(47): p. 44817-25.

98.   Mayer, M.P. and B. Bukau, *Hsp70 chaperones: cellular functions and molecular mechanism.* Cell Mol Life Sci, 2005. **62**(6): p. 670-84.

99.   Glover, J.R. and S. Lindquist, *Hsp104, Hsp70, and Hsp40: A novel chaperone system that rescues previously aggregated proteins.* Cell, 1998. **94**(1): p. 73-82.

100. Grimminger-Marquardt, V. and H.A. Lashuel, *Structure and function of the molecular chaperone Hsp104 from yeast.* Biopolymers, 2010. **93**(3): p. 252-76.

101. Park, *The effect of MG132, a proteasome inhibitor on HeLa cells in relation to cell growth, reactive oxygen species and GSH.* Oncology Reports, 2009. **22**(01).

102. Nonaka, T., et al., *Prion-like properties of pathological TDP-43 aggregates from diseased brains.* Cell Rep, 2013. **4**(1): p. 124-34.

103. Walsh, D.M. and D.J. Selkoe, *Oligomers on the brain: the emerging role of soluble protein aggregates in neurodegeneration.* Protein Pept Lett, 2004. **11**(3): p. 213-28.

104. Liu, Y.C., P.M. Chiang, and K.J. Tsai, *Disease animal models of TDP-43 proteinopathy and their pre-clinical applications.* Int J Mol Sci, 2013. **14**(10): p. 20079-111.

105. Shaw, G., et al., *Preferential transformation of human neuronal cells by human adenoviruses and the origin of HEK 293 cells.* FASEB J, 2002. **16**(8): p. 869-71.

106. Shorter, J., *The mammalian disaggregase machinery: Hsp110 synergizes with Hsp70 and Hsp40 to catalyze protein disaggregation and reactivation in a cell-free system.* PLoS One, 2011. **6**(10): p. e26319.

# Appendices

Appendix A: Supplementary Figures
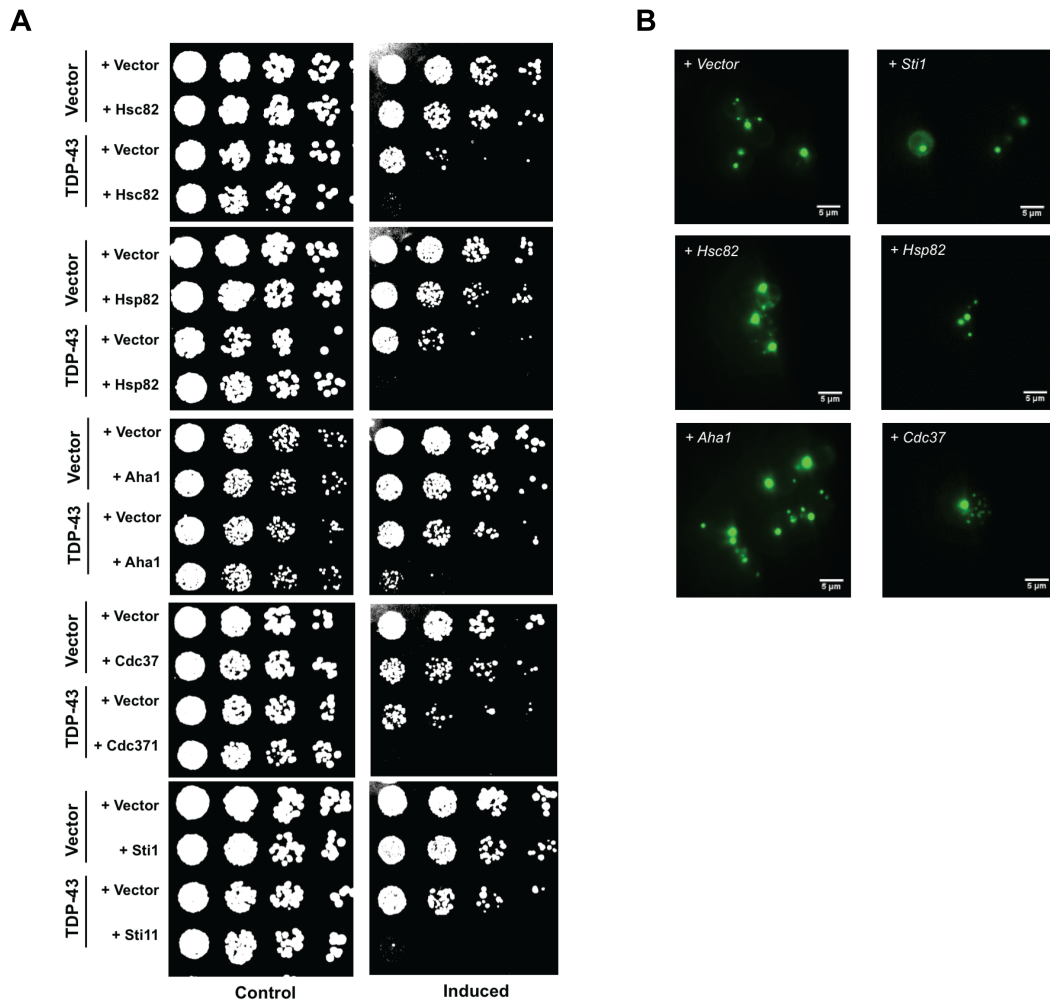
Figure 24: Hsp90 and co-chaperones and TDP-43 interaction in yeast strain W303. **A** Spotting assays and **B** Fluorescence microscopy of TDP-43-expressing wild type cells overexpressing Hsc82, Hsp82, Aha1, Cdc37, and Sti1.
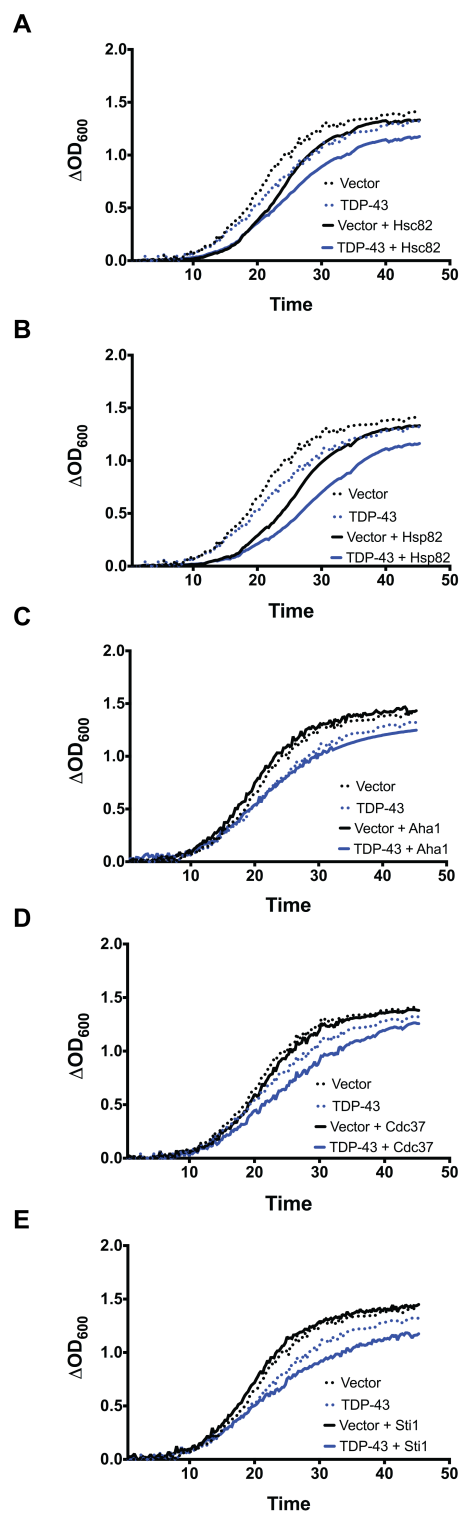
Figure 25: Growth curve assays of Hsp90 and co-chaperones and TDP-43 interaction in yeast strain W303. A Hsc82. **B** Hsp82. **C** Aha1. **D** Cdc37. **E** Sti1.
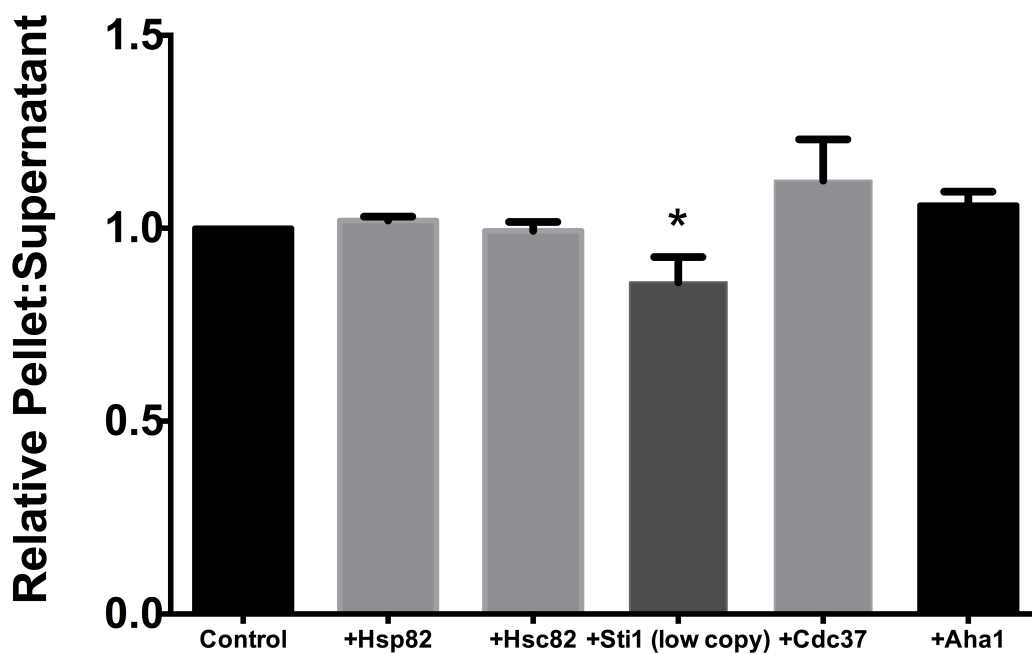
Figure 26: Statistical analysis of the sedimentation assay of Hsp90 and co-chaperones. Shown are the changes in TDP-43 pellet-to-supernatant ratio of cells overexpressing high copy Hsp82, Hsc82, Cdc37, Aha1, and low copy Sti1. *=significance level of p=0.01.

A

B

C
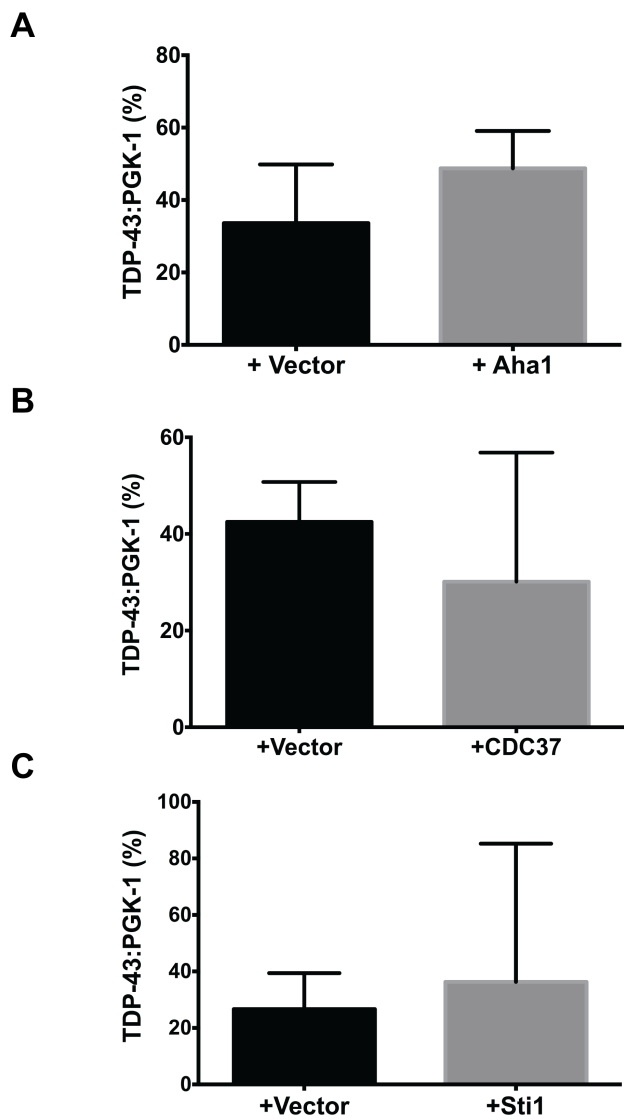
Figure 27: TDP-43 protein expression level in Hsp90 co-chaperones. A Aha1. **B** Cdc37. **C** Sti1.

Curriculum Vitae

Name: Lilian Tsai-Wei Lin

Post-secondary   National Taiwan University
Education and   Taipei, Taiwan
Degrees: 2009-2013 B.Sc.

                      RWTH Aachen University
                      Aachen, Germany
                      2013-2015 M.Sc.

                      The University of Western Ontario
                      London, Ontario, Canada
                      2016-2017 M.Sc.

Honours and   Western Graduate Research Scholarship
Awards: 2016

Related Work   Intern
Experience   Institute of Biological Sciences, Academia Sinica
                      2014

Publications:
J. W. Wu, C.Y. Kao, Lilian T. W. Lin, W. S. Wen, J. T. Lai, Steven S.-S. Wang (2013). Human YD-Crystallin Aggregation Induced by Ultraviolet C Irradiation is Suppressed by Resveratrol. Biochemical Engineering Journal. doi:10.1016/j.bej.2013.03.014

W. L. Chou, Lilian T. W. Lin, C. Y. Kao, Y. Y. Shih, C. T. Li, W. B. Tsai, and Steven S.S. Wang (2014). Aggregation Behavior of Casein is Correlated with the Type of Glycation-Inducing Agent. Journal of the Taiwan Institute of Chemical Engineers. doi:10.1016/j.jtice.2013.08.004

Chang, Chih-Kai, Wei-An Chen, Chao-Yu Sie, Shen-Chieh Lin, Lilian Tsai-Wei Lin, Ta-Hsien Lin, Cheng-Che Hsu, and Steven S.-S. Wang (2015). Investigating the Effects of Plasma Pretreatment on the Formation of Ordered Aggregates of Lysozyme. Colloids and Surfaces B: Biointerfaces: 154-61. doi:10.1016/j.colsurfb.2014.12.017

Ishtikhar, M., Khan, A., Chang, C. K., Lin, L. T., Wang, S. S., & Khan, R. H. (2015). Effect of Guanidine hydrochloride and Urea on the interaction of 6-thioguanine with

human serum albumin: A spectroscopic and molecular dynamics based study. J Biomol Struct Dyn, 1-38. doi:10.1080/07391102.2015.1054433

F. Werheid, H. Azzedine, E. Zwerenz, A. Bozkurt, M. J. Moeller, L. Lin, M. Mull, M. Häusler, J. B. Schulz, J. Weis, K. G. Claeys, Underestimated associated features in CMT neuropathies: clinical indicators for the causative gene?, Brain and Behavior, 2016; 6(4), e00451, doi: 10.1002/brb3.451

Chen PT, Chen CL, Lin LTW, Lo CH, Hu CJ, et al. (2016) Design of Peptide Substrate for Sensitively and Specifically Detecting Two Aβ-Degrading Enzymes: Neprilysin and Angiotensin-Converting Enzyme. PLoS ONE 11(4): e0153360. doi: 10.1371/journal.pone.0153360